Kinetics of Reactions of H Atoms With Methane and Chlorinated Methanes

Mikhail G. Bryukov,[†,‡] Irene R. Slagle,[†] and Vadim D. Knyazev*[,†,§]

Department of Chemistry, The Catholic University of America, Washington, D. C. 20064, and National Institute of Standards and Technology, Physical and Chemical Properties Division, Gaithersburg, Maryland 20899

Received: July 3, 2000; In Final Form: January 25, 2001

The reactions of H atoms with methane, four chlorinated methanes, and isobutene have been studied experimentally using the discharge flow/resonance fluorescence technique over wide ranges of temperatures. The rate constants were obtained in direct experiments as functions of temperature. The experimentally obtained activation energies of the reactions of H atoms with chlorinated methanes demonstrate a correlation with the enthalpies of the reactions. Transition state theory reaction models were created on the basis of ab initio calculations, the Marcus expression for correlation between reaction barriers and reaction energetics, and analysis of experimental data. It is demonstrated that the formalism based on the Marcus expression adequately describes the observed temperature dependencies of the rate constants of the overall reactions. According to the models, abstraction by H atoms of hydrogen atoms from chloromethanes is an important process accounting for significant fractions of the overall rate constants. The models result in expressions for the rate constants of Cl and H atom abstraction channels and the corresponding reverse reactions over wide ranges of temperatures.

I. Introduction

To make the incineration of industrial wastes more efficient and less hazardous, it is necessary to understand all aspects of this combustion process. Basic understanding of the incineration mechanism is especially important in the case of chlorinated hydrocarbons (CHCs), whose burning has the potential to generate products such as phosgene which are more hazardous than the CHCs themselves. Fundamental knowledge of mechanisms, specific pathways, and rate constants of important elementary reactions, including those of chlorinated hydrocarbons, is of key importance to the success of kinetic modeling of these systems.

In CHC/O_2 and $CHC/hydrocarbon/O_2$ flames, the major channels of consumption of CHCs are unimolecular decomposition and the reactions of CHCs with Cl and H atoms.[1−14] The results of numerical simulations of these complex combustion systems indicate a high sensitivity of the rates of CHC destruction and of the concentration of active species to the rates of Cl + CHC and H + CHC reactions.[1,2,5,8,10−14] The inhibitive effect of these reactions is associated with the binding of hydrogen atoms into stable HCl, which then scavenges OH radicals to form Cl atoms and water.[5,10] In fuel-rich flames, the reactions of H atoms with CHCs compete directly with the main chain-branching reaction, $H + O_2 \rightarrow OH + O$.[1,14−16]

Although the importance of the H + CHC reactions has been shown, little is known about the rates of even the chlorinated methanes, the simplest CHC reactions. There are no direct measurements of the rate constants of $H + CCl_4$ or $CHCl_3$ reported in the literature. The only experimental determination of the rate constant of the $H + CH_2Cl_2$ reaction at elevated temperatures (298−460K) is that of Combourieu et al.,[16] who used the discharge flow method with mass spectrometric detection of reactants and products. Several measurements of the rate constant of the $H + CH_3Cl$ reaction are reported in the literature,[17−21] including three studies where temperature dependencies are reported.[17−19] However, the results of these studies are in substantial disagreement with each other, with rate coefficients differing by more than an order of magnitude. In refs 16 and 18−21, high initial concentrations of H atoms were used (10^{13}−10^{15} atoms cm^{-3}), which could result in errors in the rate measurement due to the effects of secondary reactions (see Discussion).

To firmly establish the rate coefficients of H + CHC reactions, experiments must be conducted with very low initial concentrations of hydrogen atoms ($<10^{11}$ atoms cm^{-3}), thus ensuring the absence of any complications due to fast secondary reactions. To this end, we have constructed a heatable discharge flow reactor with resonance fluorescence detection of H atoms. This technique has excellent sensitivity to hydrogen atoms (detection limit $<10^8$ atoms cm^{-3}), allowing us to make rate measurements with the necessary low initial concentrations. Here we report the results of our first study, the reactions of H atoms with the simplest members of the class of chlorinated hydrocarbons, chlorinated methanes

$$H + CCl_4 \rightarrow HCl + CCl_3 \text{ (297−904 K)} \quad (1)$$

$$H + CHCl_3 \rightarrow \text{products (455−854 K)} \quad (2)$$

$$H + CH_2Cl_2 \rightarrow \text{products (498−787 K)} \quad (3)$$

$$H + CH_3Cl \rightarrow \text{products (586−839 K)} \quad (4)$$

(Numbers in parentheses indicate the experimental ranges of the current work.) In a series of ancillary experiments, two reactions whose rate constants are well established[22−28]

$$H + CH_4 \rightarrow H_2 + CH_3 \text{ (748−1054 K)} \quad (5)$$

$$H + \textit{iso}\text{-}C_4H_8 \rightarrow \textit{tert}\text{-}C_4H_9 \text{ (299−503 K)} \quad (6)$$

were also studied in order to validate the experimental techniques used.

* Corresponding author. E-mail: knyazev@cua.edu.
† The Catholic University of America.
‡ Due to different methods of transliteration from Cyrillic alphabet, this name has also been spelled as Mikhail G. Brioukov.
§ National Institute of Standards and Technology.

10.1021/jp0023359 CCC: $20.00
Published on Web 03/02/2001

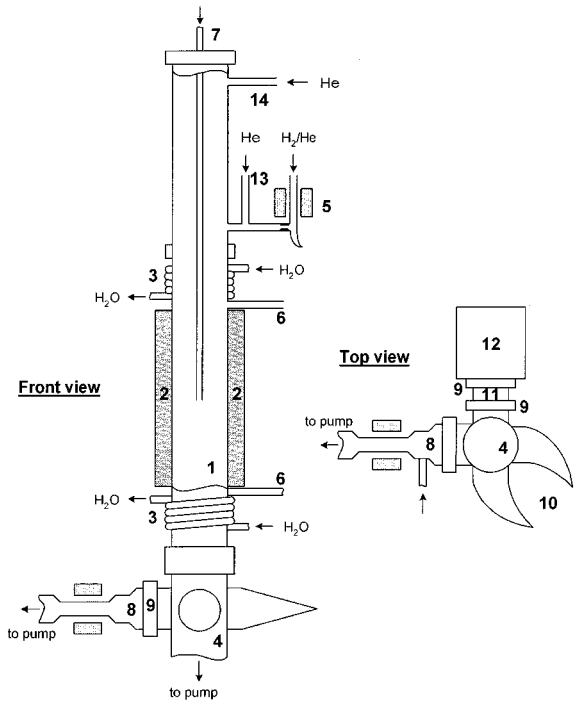

Figure 1. Schematic of the discharge flow/resonance fluorescence apparatus. Equipment parts are the following: reactor tube (1), heater (2), cooling coils (3), optical detection assembly (4), atom-generating microwave discharge (5), pressure measurement outlets (6), moveable injector (7), discharge flow lamp (8), MgF_2 windows (9), light traps (10), oxygen optical filter (11), photomultiplier tube (12), and carrier gas inlets (13 and 14).

This article is organized as follows. Section I (current) is an introduction. Experimental method, procedures, and results are reported in section II. In section III, quantum chemical calculations and the transition state theory modeling of reactions 1−5 are presented. Modeling is used to separate the experimentally determined overall rate constants into those of H and Cl atom abstractions. The results are discussed in section IV.

II. Experimental Section

Rate constant measurements were conducted in a heatable tubular flow reactor under pseudo-first-order conditions with a large excess of molecular substrate. H atoms were detected by resonance fluorescence and their decay measured as a function of contact time over a wide range of experimental conditions.

II.1. Experimental Apparatus. A schematic of the experimental apparatus is shown in Figure 1. The tubular quartz or Pyrex[29] flow reactor (1), resistively heated by a Nichrome[29] wire heater (2), was attached to a Pyrex six-way cross that served as the base of the optical detection system. Pressure in the reactor was monitored through outlets (6) positioned at the ends of the heated zone.

The viscous pressure drop in the heated zone of the reactor was obtained by measuring the difference in pressure values obtained upstream and downstream of the heated zone and by subsequent interpolation. A typical value of the viscous pressure drop in the working part of the heated zone was 4−8 Pa (0.03−0.15 Torr).

Temperature profiles along the reactor were measured with a movable thermocouple and referenced to a readout of a fixed thermocouple positioned in the heater. The uniformity of the temperature profiles in the working part of the heated zone (20−30 cm in length) was at least 5 K (maximum temperature differences were 5 K at the highest temperature used and less at lower temperatures).

Various aspects of the discharge flow technique of measuring rate constants of gas phase chemical reactions have been extensively discussed in the literature.[30−33] These discussions are not repeated here. Care was taken to ensure that, under all experimental conditions used in the current work, the plug-flow approximation was valid. The only exception to the plug flow approximation was the minor, although non-negligible, contribution of axial diffusion of H atoms. Corrections for the axial diffusion had to be introduced into the experimentally obtained atom decay rates (vide infra).

Three reactors were used in these experiments: a quartz reactor with an internal diameter (i.d.) of 1.93 cm, a Pyrex[29] reactor with i.d. = 2.19 cm, and a Pyrex reactor with i.d. = 4.66 cm. The reactor surface, the surface of the movable injector, and the inside of the discharge tube were treated to reduce heterogeneous loss of H atoms first by soaking in a 5% aqueous solution of ammonium bifluoride for 30 min and then by the method of Sepehrad et al.[34] The resultant values of the first-order wall loss rate constant, k_w, were always below 30 s^{-1}. Typical values of k_w were ∼4 s^{-1} for the Pyrex reactors and 12−25 s^{-1} for the quartz reactor. Reactors of different diameters were used to rule out potential contributions of heterogeneous reactions to the rate constant values obtained in the experiments (vide infra).

H atoms were generated by a 2.45 GHz microwave discharge (5) in a H_2/He mixture. Hydrogen atoms formed in the discharge area were carried through the reactor by a flow of helium injected through inlet (13), and their concentration was monitored by resonance fluorescence in the detection zone (4). An additional flow of helium was introduced in the back section of the reactor (inlet 14) to eliminate any stagnant "dead volume." The molecular substrate ($C_xH_yCl_z$) was introduced through a quartz movable injector (7).

H atom resonance fluorescence (Lyman-α, 121.6 nm) was induced by light from a discharge flow resonance lamp[35,36] and detected by a solar blind photomultiplier (EMR model 542-G-09[29]). A molecular oxygen optical filter (11) (18.7 kPa (140 Torr) of O_2, optical path length 3 cm)[37] effectively cut off radiation at all wavelengths in the range corresponding to the peak of the photomultiplier sensitivity (115−170 nm) except for the four narrow gaps in the spectrum of O_2 (between 115 and 122 nm), one of which coincides with the Lyman-α hydrogen atom line (121.6 nm).[36]

The sensitivity of the atom detection system to H atoms was determined by titration with NO_2 (rate constant of the H + NO_2 reaction is 1.4×10^{-10} cm^3 $molecule^{-1}$ s^{-1}).[38] Typical concentrations at which the fluorescence signal was equal to the scattered light from the discharge flow lamp were ∼10^9 atom cm^{-3}. The sensitivity limit (defined by a signal-to-noise ratio of unity) was <10^8 atom cm^{-3}. In the titration experiments, relatively high concentrations of H atoms had to be used (∼10^{12} atoms cm^{-3}). Such concentrations caused some degree of self-absorption of light at the Lyman-α line, which resulted in a nonlinear dependence (saturation) of the resonance fluorescence signal on the atom concentration. Thus, the calibration of the H atom signal based on measuring the decrease in fluorescence signal upon the addition of a small flow of NO_2 to the reactor yielded underestimated values of sensitivity coefficients (defined as the ratio of signal to H concentration). Therefore, the values of the initial concentrations of H atoms used in the experiments to determine the rate constants of reactions 1−6 (listed in Table 1) are somewhat overestimated and should be understood as upper limits to $[H]_0$.

TABLE 1: Conditions and Results of Experiments to Measure Rate Constants of the Reactions of H Atoms with Chlorinated Methanes, Methane, and Isobutene

N^o [a]	T/K	P/kPa[b]	$[C_xH_yCl_z]$ range/ 10^{12} molecules cm^{-3}	k_0/s^{-1} [c]	V/cm s^{-1} [d]	$[H]_0/10^{10}$ molecules cm^{-3}	$((k'_{OBS}D/V^2))_{max}$	k_i[e]$/10^{-15}$ cm^3 molecules^{-1} s^{-1}
				H + CCl_4 → HCl + CCl_3				
1−1*	297	0.780−0.884	1400−3540	0.1 ± 0.9	319−353	3.8	0.066	7.04 ± 0.39
1−2$^+$	297	0.380−0.403	475−7285	2.0 ± 3.9	627−656	7	0.082	8.91 ± 0.94
1−3$^+$	325	0.388−0.403	779−6690	2.1 ± 6.0	276−654	2	0.165	15.2 ± 1.7
1−4$^+$	346	0.404−0.407	190−1351	−1.1 ± 3.8	739−779	5	0.045	28.1 ± 4.8
1−5$^+$	363	0.399−0.405	200−2744	0.7 ± 3.9	783−809	7	0.141	49.2 ± 2.7
1−6*	381	0.775−0.827	502−1350	0.9 ± 5.2	428−452	3.6	0.144	51.1 ± 5.9
1−7$^+$	399	0.400−0.404	180−1920	−1.4 ± 7.5	850−870	4	0.195	102.4 ± 8.7
1−8*	437	0.397−0.411	64.7−970	−0.1 ± 7.8	658−674	3	0.262	139 ± 12
1−9$^+$	456	0.399−0.400	198−1080	8.7 ± 19.8	2923−2981	3	0.025	176 ± 29
1−10$^+$	503	0.387−0.407	329−1250	−0.6 ± 12.4	1314−1383	2	0.198	310 ± 18
1−11$^+$	561	0.373−0.408	119−773	−4.3 ± 17.8	1594−1651	3	0.142	647 ± 45
1−12	606	0.400−0.405	63.0−435	−8.3 ± 32.0	1909−2131	10	0.204	1090 ± 130
1−13	690	0.400−0.408	24.5−183.9	0.7 ± 11.3	1801−2196	8	0.198	1760 ± 130
1−14	754	0.360−0.377	19.4−119.9	1.2 ± 5.6	2185−2253	2	0.171	3113 ± 87
1−15	806	0.405−0.412	7.15−112.8	12 ± 22	2534−3788	10	0.092	4080 ± 370
1−16	854	0.392−0.401	9.82−115.8	30 ± 29	2476−2565	2	0.255	4570 ± 460
1−17	904	0.396−0.408	20.2−94.4	−16 ± 21	2755−3658	7−10	0.137	5920 ± 430
1−18	904	0.396−0.400	22.8−73.9	5 ± 32	3613−3633	3	0.107	5670 ± 820
				H + $CHCl_3$ → products				
2−1*	417	0.743−0.825	511−2020	0.5 ± 4.0	394−436	2.4	0.138	23.0 ± 3.1
2−2*	437	0.781−0.843	450−2020	−0.7 ± 3.3	465−505	2.5	0.149	36.7 ± 2.7
2−3$^+$	455	0.396−0.403	602−2267	0.2 ± 4.0	840−1050	1	0.117	39.8 ± 2.9
2−4*	483	0.377−0.431	204−1790	0.0 ± 2.8	738−736	2.3	0.232	69.7 ± 2.7
2−5$^+$	503	0.401−0.404	563−2946	−14.5 ± 14.8	2267−2552	3	0.061	91.1 ± 7.9
2−6$^+$	563	0.391−0.401	107−1473	−17 ± 18	1355−2467	4	0.118	196 ± 22
2−7	629	0.391−0.397	167−632	−5.5 ± 10.0	2157−2369	8	0.083	338 ± 27
2−8	721	0.379−0.405	63.3−290	13 ± 18	1238−2865	4	0.086	1000 ± 120
2−9	807	0.385−0.399	69−284	8 ± 23	2488−2641	5	0.175	1390 ± 160
2−10	854	0.395−0.404	7.2−153	4 ± 13	1906−2584	3	0.137	1830 ± 140
2−11	854	0.384−0.393	24.8−148	4 ± 18	2521−2666	3	0.151	2070 ± 180
				H + CH_2Cl_2 → products				
3−1*	491	0.787−0.833	819−2590	1.8 ± 4.7	488−551	4.4	0.151	25.8 ± 2.8
3−2	498	0.395−0.408	887−3100	5 ± 11	880−1183	4.0	0.162	32.0 ± 5.9
3−3	530	0.389−0.400	232−2030	−4 ± 6	857−1018	3	0.143	42.4 ± 5.4
3−4*	556	0.371−0.400	250−1790	2.0 ± 6.8	836−853	2	0.220	61.6 ± 6.6
3−5	583	0.395−0.401	258−1630	10 ± 17	1113−1292	4	0.196	95.4 ± 17.5
3−6	633	0.391−0.397	136−986	7 ± 14	1218−1339	4	0.190	164 ± 24
3−7	684	0.396−0.404	126−836	11 ± 31	1702−1824	2.5	0.190	315 ± 61
3−8	708	0.392−0.401	197−811	−12 ± 12	2242−2460	1.5	0.118	335 ± 22
3−9	735	0.397−0.415	92.4−804	−5 ± 34	2048−2158	4	0.219	438 ± 75
3−10	787	0.399−0.416	55.6−530	11 ± 12	2117−2240	4	0.198	697 ± 46
3−11	787	0.395−0.408	89.6−731	−17 ± 23	3043−3281	4	0.130	626 ± 56
				H + CH_3Cl → products				
4−1*	586	0.753−0.824	490−2530	−0.7 ± 5.1	601−648	1.4	0.126	22.4 ± 3.3
4−2*	615	0.371−0.425	209−3400	−2.0 ± 7.0	934−959	2.3	0.211	34.7 ± 4.1
4−3	633	0.381−0.428	715−2500	−5.6 ± 8.9	1374−1640	1.8	0.128	45.7 ± 5.7
4−4	684	0.407−0.408	388−1420	−12.8 ± 9.6	1585−1726	2.6	0.088	86.0 ± 10.5
4−5	708	0.391−0.415	173−1730	−4.9 ± 6.7	1725−1903	1.6	0.126	106.9 ± 7.3
4−6	735	0.396−0.400	300−1190	−15 ± 14	2009−2195	3.3	0.087	137 ± 19
4−7	787	0.401−0.407	279−922	−21 ± 13	2036−2164	2.5	0.138	257 ± 23
4−8	839	0.403−0.405	143−505	3 ± 15	2148−2257	6	0.118	379 ± 47
4−9	839	0.392−0.420	95.2−951	−12 ± 16	3196−3370	3	0.086	336 ± 31
				H + CH_4 → H_2+CH_3				
5−1*	748	0.747−0.816	636−3290	−2.1 ± 4.1	791−817	1.8	0.152	25.9 ± 2.0
5−2	806	0.769−0.829	934−3220	12 ± 11	1231−1257	4.9	0.145	51.3 ± 5.2
5−3	855	0.403−0.433	719−2820	20 ± 15	1970−2005	8.7	0.169	84.2 ± 9.6
5−4	889	0.400−0.427	469−3610	−29 ± 16	1914−2181	4.4	0.222	103.0 ± 8.0
5−5	905	0.389−0.428	418−2470	12 ± 16	1971−2009	5.8	0.256	137 ± 11
5−6	956	0.399−0.425	239−1450	23 ± 14	1839−1870	5.3	0.246	192 ± 16
5−7	1005	0.796−0.828	172−1454	33 ± 21	1895−1935	3.7	0.213	270 ± 24
5−8	1054	0.821−0.859	216−1550	19 ± 14	2205−2249	8.2	0.234	380 ± 18
				H + *iso*-C_4H_8 → *tert*-C_4H_9				
6−1	299	0.133	3.15−14.6	4.6 ± 7.0	576	9	0.23	3880 ± 460
6−2	301	0.128	4.49−14.7	4 ± 5	591	3	0.23	3930 ± 700
6−3	346	0.380−0.389	16.4−73.6	9.1 ± 13.7	2215−2333	3	0.057	6100 ± 360
6−4	399	0.395−0.396	6.87−41.7	−0.1 ± 22.9	2247−2553	2	0.049	7610 ± 1220
6−5	456	0.400	10.9−75.9	−7.5 ± 19.1	2697	3	0.096	8800 ± 0510
6−6	503	0.395−0.399	9.18−44.3	−2.3 ± 26.6	2961−2989	1	0.063	10700 ± 1000

[a] Experiment number. Pyrex reactor with internal diameter with i.d. = 4.66 cm was used in experiments marked with *, Pyrex reactor with i.d. = 2.19 cm was used in experiments marked with +, and quartz reactor with i.d. = 1.93 cm was used in unmarked experiments. [b] 1 kPa = 7.5006 Torr. Minor variations in pressure are due to changes in flow conditions upon addition of large flows of molecular substrate ($C_xH_yCl_z$). [c] Zero-abscissa intercept on the k' vs $[C_xH_yCl_z]$ dependence (see discussion of formula IV in the text). [d] Bulk flow velocity range. Minor variations in flow velocity are due to changes in flow conditions upon the addition of large flows of molecular substrate ($C_xH_yCl_z$). Also, in some experiments, large variations of flow velocity were introduced intentionally. [e] Error limits represent statistical uncertainties and are reported as 2σ. Maximum estimated systematic uncertainties are 8% of the rate constant value (see text).

Molecular substrates ($C_xH_yCl_z$) were stored undiluted in Pyrex[29] reservoirs. Flows of these reagents into the reactor were determined by measuring the pressure drop in a calibrated volume over time. These pressure measurements were performed with a differential capacitance manometer (MKS Instruments model 223BD-00010ACU).[29] The independence of the measured flows of the surface-to-volume ratio of the calibrated volume was verified to ensure the absence of interference from heterogeneous absorption and desorption processes on the walls of vacuum manifold. Flows of molecular hydrogen to the atom-producing discharge were measured in a similar way. It was found that the typical dissociation efficiency of the discharge was ≈20%. This resulted in the concentrations of undissociated H_2 in the reactor being approximately a factor of 2−3 higher than the initial H atom concentrations.

II.2. Reaction Rate Measurements and Results. All experiments to measure the rate constants of reactions 1−6 were conducted under the conditions of large excess of molecular substrate ($35 \le [C_xH_yCl_z]/[H]_0 \le 3.4 \times 10^5$). Initial concentrations of H atoms in the detection zone were in the range of $(1-10) \times 10^{10}$ atoms cm^{-3}. (These values of $[H]_0$ should be understood as upper limits to the actual concentrations of hydrogen atoms since the calibration procedure underestimated the calibration coefficient values, as described in subsection II.1.) Exact knowledge of H atom concentrations is not needed for determination of rate constants because the experiments were conducted under pseudo-first-order conditions. Rate constants of heterogeneous loss of H atoms on the walls of the reactor and the movable injector were regularly measured (in the absence of molecular substrate). In these measurements, the time of contact between H atoms generated in the discharge and the walls was varied by changing the flow velocity (by means of switching flow of helium carrier gas between inlet 14 and the movable injector 7 (Figure 1) at various positions of the latter) without changing the conditions in the discharge and monitoring the resultant changes in the signal of H atoms in the detection zone. The rate constants for H atom wall loss were typically in the range of 4−25 s^{-1} and always less than 30 s^{-1}.

The time of contact between the molecular substrate and H atoms was varied by changing the position of the movable injector. Under the experimental conditions used, plug flow conditions are satisfied (except for a required correction for axial diffusion, vide infra), and increments of contact time can be obtained by dividing the corresponding changes in the length of the contact zone by the bulk flow velocity, V. The tip of the movable injector was always kept within the constant temperature zone of the reactor.

The total signal (counts s^{-1}) detected by the photomultiplier consisted of three components: the fluorescence of H atoms (S_H), the photomultiplier dark current (less than 1 count s^{-1}), and the scattered light originating from the resonance lamp and reflected by the walls of the detection system (typically, ∼30 counts s^{-1}). The contributions from the dark current and the scattered light were measured directly in the absence of H atoms but with the molecular substrate present (to account for possible absorption of the scattered light) and later subtracted from the total signal to obtain S_H.

The effective first-order rate constant values, k'_{OBS}, were obtained from least-squares-fits of the H atom fluorescence signal S_H to the equation

$$\ln(S_H) = \text{constant} - k'_{OBS} x V^{-1} \qquad \text{(I)}$$

where x is the distance between the tip of the movable injector and the detection zone and V is the bulk flow velocity in the reactor. Examples of experimentally obtained $\ln(S_H)$ versus x dependencies are presented in Figure 2. The observed values of k'_{OBS} were corrected for the axial and radial diffusion of H atoms via the formula[30,33,39]

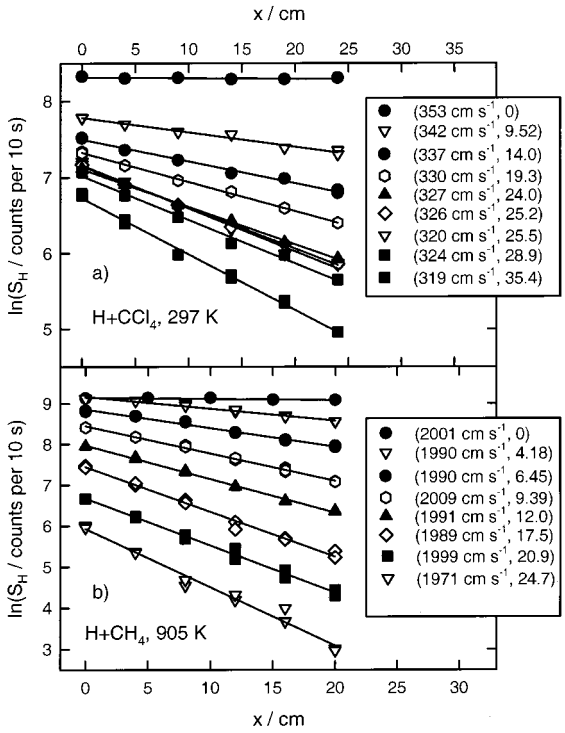

Figure 2. Examples of experimentally obtained $\ln(S_H)$ vs x dependencies. Data from experiments 1-1 and 5-5 (see Table 1). Numbers in parentheses are flow velocities and concentrations of the CH_yCl_z substrate (in 10^{14} molecules cm^{-3}).

$$k' = k'_{OBS}\left(1 + \frac{k'_{OBS} D}{V^2} + \frac{k'_{OBS} R^2}{48D}\right) \qquad \text{(II)}$$

where D is the diffusion coefficient of H atoms in He and R is the reactor radius. The values of D were taken from the

$$D = 1.790(T/273\ \text{K})^{1.77}\ \text{cm}^2\ \text{s}^{-1}\ (P = 1.01\ \text{bar}) \qquad \text{(III)}$$

dependence derived by Krasnoperov et al.[40] based on the results of experiments and calculations reported in refs 41−43. This correction for diffusion never exceeded 21% of the final value of k'.

The bimolecular rate constants of reactions 1−6 were obtained from the slopes of the linear dependencies of k' on the concentration of substrate, $[C_xH_yCl_z]$

$$k' = k_i[C_xH_yCl_z] + k_0 \qquad \text{(IV)}$$

Here, k_i is the bimolecular rate constant of the reaction under study ($i = 1-6$), and k_0 is the zero-abscissa intercept of the k' versus $[C_xH_yCl_z]$ dependence. The conditions and results of experiments to determine the values of rate constants of reactions 1−6 are presented in Table 1.

The k_0 intercept appears due to the non-negligible wall losses of H atoms on the surfaces of the reactor and the movable injector. k_0 can acquire both positive and negative values. If the probability of H atom loss upon collision with the wall of the movable injector is similar to or higher than that for the collision with the reactor wall, k_0 should be negative. However, if heterogeneous loss is significantly more efficient on the reactor wall than on the injector surface, or if this heterogeneous

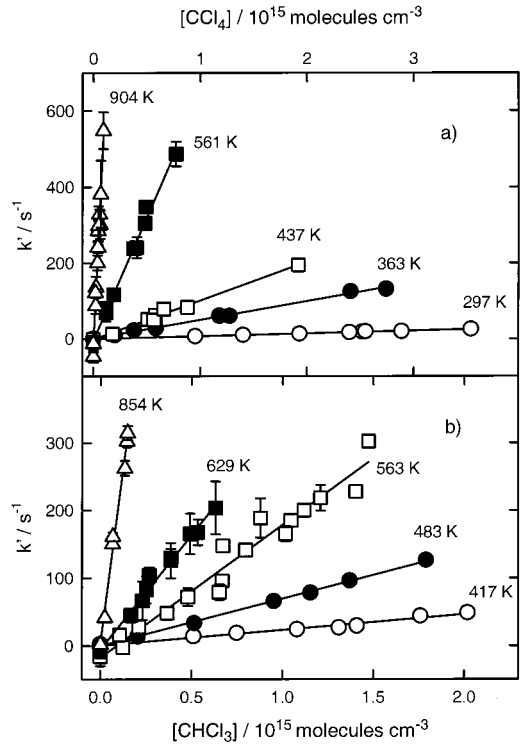

Figure 3. Examples of experimentally obtained k' vs $[CCl_4]$ (a) and k' vs $[CHCl_3]$ (b) dependencies. Experimental temperatures are indicated on the plots.

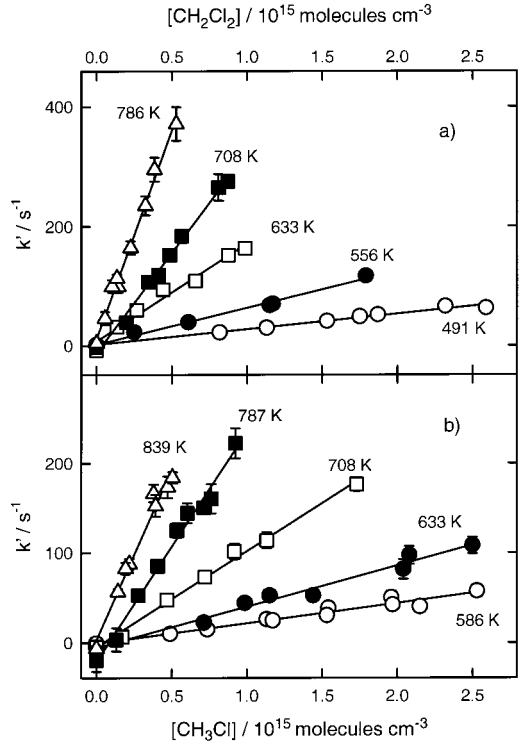

Figure 4. Examples of experimentally obtained k' vs $[CH_2Cl_2]$ (a) and k' vs $[CH_3Cl]$ (b) dependencies. Experimental temperatures are indicated on the plots.

loss is enhanced by the presence of molecular substrate in the reactor (wall reaction with the adsorbed substrate), k_0 can acquire positive values. In the current study, both positive and negative values of k_0 were observed. However, these values of k_0 were minor compared with the first term in eq IV (see Table 1), and uncertainties in k_0 were comparable with the k_0 values. Examples

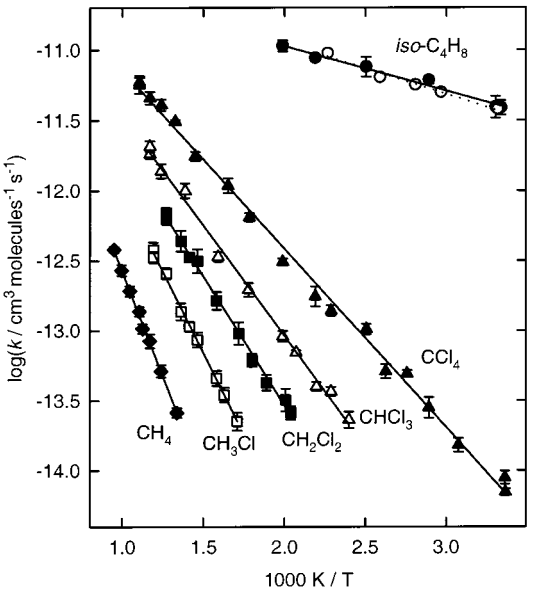

Figure 5. Experimental temperature dependencies of the rate constants of reactions 1−6. Symbols are experimental data points: filled triangles, reaction 1; open triangles, reaction 2; filled squares, reaction 3; open squares, reaction 4; diamonds, reaction 5; filled circles, reaction 6; open circles, data on reaction 6 from Harris and Pitts.[28] Solid lines are Arrhenius fits of data obtained in the current work (formulas 5−10). The dotted line is the temperature dependence of k_6 from ref 28.

of experimentally obtained k' versus $[C_xH_yCl_z]$ dependencies are presented in Figures 3 and 4.

Heterogeneous reactions of H atoms with the $C_xH_yCl_z$ substrate adsorbed on the reactor wall could potentially influence the observed rate of H atom decay, k'. If adsorption of substrate is saturated, this effect would be manifested only by positive values of k_0, and the values of k_i obtained would not be affected. If, however, the adsorption is not saturated but increases with the concentration of substrate, the contribution of such a heterogeneous reaction can influence the slope of the k' versus $[C_xH_yCl_z]$ dependence. Here, there are two possibilities. First, the dependence of the surface density of substrate on its concentration in the gas phase is nonlinear. In this case, a hypothetical heterogeneous component to the observed H atom decay rate would exhibit a nonlinear dependence on $[C_xH_yCl_z]$. The second case is encountered if the density of the adsorbed substrate increases linearly with its gas-phase concentration. In this case, the observed k' versus $[C_xH_yCl_z]$ dependencies are expected to be linear, as in the case of a purely gas-phase reaction.

To ensure that the measured rates of H atom decay in the presence of $C_xH_yCl_z$ represent the homogeneous reactions 1−5, we conducted the experiments with reactors of different internal diameters (1.93−4.66 cm) possessing different surface-to-volume ratios. The experimentally obtained values of rate constants were independent of the reactor used (Table 1). This independence, as well as the linearity of the observed k' versus $[C_xH_yCl_z]$ dependencies, indicates the absence of any significant effects of potential heterogeneous reactions on the values of the rate constants.

The rate constants of reactions 1−6 demonstrate no dependence on pressure or initial concentration of H atoms within the experimental ranges. The observed pressure independence is expected since the mechanisms of reactions 1−5 are expected to be those of atom abstraction and reaction 6 is expected to be in its high-pressure limit under the experimental conditions used.[44] The rate constants display no dependence on the initial

H atom concentration, indicating the absence of any influence of potential secondary reactions on the kinetics of H atoms, as can be expected due to the low values of $[H]_0$ used ($[H]_0 = (1-10) \times 10^{10}$ atoms cm^{-3}).

The rate constants of reactions 1−6 exhibit positive temperature dependencies (Figure 5) that can be represented with Arrhenius expressions within their corresponding experimental temperature ranges

$$k_1 = (1.36 \pm 0.31) \times 10^{-10} \exp(-2937 \pm 92\ \mathrm{K}/T)\ \mathrm{cm^3\ molecule^{-1}\ s^{-1}} (297-904\ \mathrm{K}) \quad \text{(V)}$$

$$k_2 = (1.33 \pm 0.43) \times 10^{-10} \exp(-3640 \pm 154\ \mathrm{K}/T)\ \mathrm{cm^3\ molecule^{-1}\ s^{-1}} (417-854\ \mathrm{K}) \quad \text{(VI)}$$

$$k_3 = (1.43 \pm 0.50) \times 10^{-10} \exp(-4250 \pm 184\ \mathrm{K}/T)\ \mathrm{cm^3\ molecule^{-1}\ s^{-1}} (491-787\ \mathrm{K}) \quad \text{(VII)}$$

$$k_4 = (2.24 \pm 0.75) \times 10^{-10} \exp(-5394 \pm 202\ \mathrm{K}/T)\ \mathrm{cm^3\ molecule^{-1}\ s^{-1}} (586-839\ \mathrm{K}) \quad \text{(VIII)}$$

$$k_5 = (2.55 \pm 0.89) \times 10^{-10} \exp(-6874 \pm 267\ \mathrm{K}/T)\ \mathrm{cm^3\ molecule^{-1}\ s^{-1}} (748-1054\ \mathrm{K}) \quad \text{(XI)}$$

$$k_6 = (4.57 \pm 1.32) \times 10^{-11} \exp(-729 \pm 92\ \mathrm{K}/T)\ \mathrm{cm^3\ molecule^{-1}\ s^{-1}} (299-503\ \mathrm{K}) \quad \text{(X)}$$

The error limits in expressions V−X represent uncertainties of the fits only and are reported as 2σ. The lowest temperatures used were determined either by ambient temperature or by the impracticality of measuring rate constants that are significantly lower than 10^{-14} cm^3 molecule^{-1} s^{-1}. The upper limits of the experimental temperature ranges for reactions 1−4 were determined by the observed onsets of thermal decomposition of chlorinated methanes. Decomposition reactions manifested themselves by the apparent dependencies of the observed rates of H atom decay, k', on the flow velocity inside the movable injector, which was interpreted as resulting from the reactions of H atoms with the decomposition products. At the highest temperatures used in studies of reaction 1−4, the absence of any potential effects of thermal decomposition of chlorinated substrate was verified by measuring the rate constants twice with flow velocities through the movable injector differing by at least a factor of 2.

The sources of error in the measured experimental parameters such as temperature, pressure, flow rate, signal count, etc. were subdivided into statistical and systematic. Statistical uncertainties were estimated for parameters statistical in physical nature (for example, signal count). The estimate of possible systematic errors was based on the finite accuracy of the equipment and on the uncertainty in the H atom diffusion coefficient.[40] The uncertainties of the measured experimental parameters were propagated to the final values of the rate constants using different mathematical procedures for propagating systematic and statistical uncertainties.[45] The error limits of the experimentally obtained values reported in this work (Table 1) represent 2σ statistical uncertainty. The maximum estimated systematic uncertainty is 8% of the rate constant value.

Gases used the experiments were obtained from MG Industries[29] (He, >99.999%), Aldrich[29] (CH_2Cl_2, >99.9%; $CHCl_3$, >99.9%; CCl_4, >99.9%), and Matheson[29] (*iso*-C_4H_8, >99%; CH_4, >99.99%; CH_3Cl, >99.5%; O_2 > 99.6%). All gases except helium were purified by vacuum distillation prior to use. Helium was purified by passing through liquid nitrogen cooled traps. To verify that no potential impurities in methane or chlorinated methanes could affect the measured rate constants, we analyzed these gases for potential contaminants by gas chromatography. A Shimadzu GC-9A gas chromatograph[29] was used in these analyses. After purification by vacuum distillation, the purity of all chloromethanes was better than 99.98%, significantly exceeding the specifications provided by the manufacturers.

III. Modeling

Rate constants of reactions 1−5 were obtained experimentally over wide temperature ranges. Nevertheless, the temperatures used in the experiments to determine the rates of each of these reactions (Table 1) are still far from covering the whole temperature range of practical interest, which extends to the temperatures of combustion, i.e., up to 2000−2500 K. Accurate extrapolation of rate constants to higher temperatures requires application of theory and modeling.

The reactions of H atoms with partially chlorinated methanes can proceed through the abstraction of both chlorine and hydrogen atoms

$$\mathrm{H + CHCl_3 \rightarrow HCl + CHCl_2} \quad \text{(2a)}$$

$$\mathrm{\rightarrow H_2 + CCl_3} \quad \text{(2b)}$$

$$\mathrm{H + CH_2Cl_2 \rightarrow HCl + CH_2Cl} \quad \text{(3a)}$$

$$\mathrm{\rightarrow H_2 + CHCl_2} \quad \text{(3b)}$$

$$\mathrm{H + CH_3Cl \rightarrow HCl + CH_3} \quad \text{(4a)}$$

$$\mathrm{\rightarrow H_2 + CH_2Cl} \quad \text{(4b)}$$

The experimental values of the rate constants of reactions 2−4 reported in Table 1 and presented in Figure 5 reflect the sums of Cl and H abstraction processes. On the basis of the experimental information obtained in this work, one cannot distinguish these different reaction channels. Therefore, modeling must be applied to separate the experimental rate constant values into those of the individual elementary reactions and to extrapolate these values to higher temperatures.

In this section, efforts on modeling of reactions 1−5 are described. This modeling was based on application of transition state theory, analysis of relationships between reaction barriers and thermochemistry, and quantum chemical calculations. A significant portion of this modeling is directed toward the estimation of the relative importance of chlorine versus hydrogen atom abstraction in reactions 2−4. First, ab initio calculations of some of the properties of the transition states are performed (subsection III.1), and the results are used to construct first approximation models. The quantitative estimation of the importance of H atom abstraction channels is then performed by an extrapolation of the experimentally obtained H abstraction rates (reaction 5, $H + CH_4$) to the cases of reactions 2−4. This extrapolation is performed within the framework of transition state theory with an application of the Marcus equation (see subsection III.2.). The rates of the Cl atom abstraction processes in reactions 2−4 are obtained by subtracting the estimated H abstraction rates (minor channels) from the experimental overall rate data. Finally, models of all channels of reactions 1−5 are created and used to predict rate constants at temperatures outside of the experimental ranges. These reaction models, including the reaction energetics, and computation of the rate constants are described in subsection III.2. As with any modeling based on statistical rate theories, the estimates of branching in reactions

2−4 must be understood as approximate and thus treated with caution. Potential uncertainties in the calculated rates of H atom abstraction arise from several sources such as the undetermined accuracy of the transition state theory, the use of the Marcus equation to predict (extrapolate) reaction barriers, and the method of vibrational frequencies adjustment (subsection III.2.). Uncertainties of the modeling results are discussed in greater detail in "Discussion" (subsection IV. 2.).

III.1. Ab Initio Study of Transition States of Reactions 1−5. Ab initio calculations are not expected, at the current state of quantum chemical theory, to produce reaction energy barrier values that are comparable in accuracy with the best experimental determinations of activation energy. Similarly, transition state properties, such as vibrational frequencies will most likely require adjustment to reproduce the experimental preexponential factors for reactions 1−5. However, ab initio calculations can be used successfully to provide other important properties of the reaction transition states, such as geometrical structures (including characteristic barrier widths important for tunneling, vide infra) and vibrational frequencies of those modes that are not significantly coupled to the reaction coordinate. Therefore, in this work, ab initio quantum chemical calculations were performed in order to obtain first-approximation-level transition state properties and reaction barrier widths.

Properties of the transition states for reactions 1, 2a, 2b, 3a, 3b, 4a, 4b, and 5 were studied. The geometry was optimized, and vibrational frequencies were obtained at the UMP2/6-31G-(d,p) level. The detailed results of ab initio calculations of transition states are presented as Supporting Information. GAUSSIAN 94[29,46] was used in all ab initio calculations. Reaction 5 has been studied before at higher levels of theory (see, for example refs 47 and 48 and references therein). The modeling part of this study, however, is primarily concerned not with the prediction of the reaction 5 rate constant from first principles but with accurate extrapolation of the experimental data and with reactivity trends in a series of similar reactions. Therefore, lower-level ab initio calculations are uniformly applied here to all reactions under study.

Tunneling can be expected to play a significant role in reactions 1−5 since they each involve a transfer of an H atom. The treatment of tunneling in the current work follows the approach used by Knyazev and Slagle[49] and Knyazev et al.[22] in their modeling of the $C_2H_3 \leftrightarrow H + C_2H_2$ and $C_2H_3 + H_2 \leftrightarrow H + C_2H_4$ reactions. Computation of under-barrier tunneling and above-barrier reflection probabilities is based on knowledge of the barrier "width." To determine the "width" parameters of reactions 1−5, we determined the shapes of the barriers of these reactions using the method of reaction path following (intrinsic reaction coordinate, IRC)[50,51] in mass-weighted internal coordinates. IRC calculations were done at the UMP2/6-31G(d,p) level for all reactions. For reaction 1, IRC calculations were also performed using the density functional B3LYP/6-31G(d,p) method. The potential energy profile along the reaction path was fitted with the Eckart function

$$V = \frac{A\xi}{(1+\xi)} + \frac{B\xi}{(1+\xi)^2} \qquad \xi = \exp\left(\frac{2\pi x}{l}\right) \qquad \text{(XI)}$$

where x is a coordinate along the reaction path, l is the "width" parameter, and parameters A and B are related to the barriers for the direct and reverse reactions E_1 and E_{-1}

$$A = \Delta E_{1,-1} = E_1 - E_{-1} \qquad B = (\sqrt{E_1} + \sqrt{E_{-1}})^2 \qquad \text{(XII)}$$

The transition probability for such a barrier can be described analytically, as shown by Eckart.[52] In the fitting process, parameter A was fixed at the value obtained from ab initio calculations, and B and l were determined from the fitting.

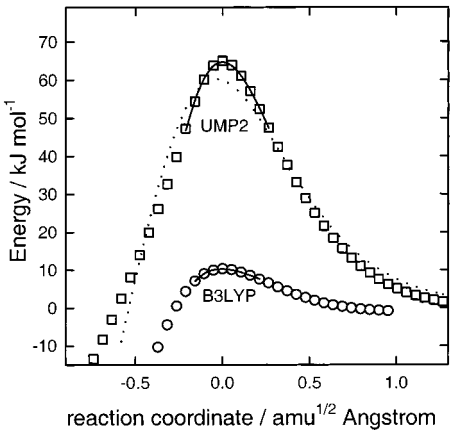

Figure 6. Potential energy profiles along IRC for reaction 1 obtained at the UMP2/6-31G(d,p) and B3LYP/6-31G(d,p) levels (squares and circles, respectively). Lines are fits with the Eckart formula (see text). The dotted line illustrates the poor quality of fit obtained by using all UMP2/6-31G(d,p)-level points with energies above that of $H + CCl_4$. The solid lines are obtained when only the top one-third of the barrier (relative to the energy of $H + CCl_4$) is used for fits.

Figure 6 presents the results of IRC calculations for reaction 1. As can be seen from the plot, the UMP2 and B3LYP methods with 6-31G(d,p) basis result in significantly different barrier heights (factor of 6 difference). Attempts to reproduce the barrier shapes with equation XI using all points with energies above those of $H + CCl_4$ result in a poor quality of fit, which is illustrated in Figure 6 by the dotted line for the case of the UMP2-level barrier. However, considering that it is the top part of the barrier that plays the most significant role in the tunneling effect, it is more important to describe this upper portion with the Eckart equation than the barrier as a whole. Thus, we limited the fitting attempts to the top one-third of the barrier, where the quality of fits was acceptable. The results are demonstrated in Figure 6 with solid lines. Although the UMP2 and the B3LYP methods yield drastically different reaction barrier heights, the values of the "width" parameter l obtained at these two levels of calculations are very close to each other for reaction 1: l(reaction 1,UMP2) = 1.685 and l(reaction 1,B3LYP) = 1.661 amu$^{1/2}$Å. A weak dependence of the barrier width parameter on the level of ab initio method used was previously demonstrated by the authors of refs 49 and 22, who found that improvement of the level of theory from UMP2 to UMP4 and spin-projected PMP4[53,54] methods did not result in significant changes of the "width" parameter l for the $C_2H_3 \leftrightarrow H + C_2H_2$ and $C_2H_3 + H_2 \leftrightarrow H + C_2H_4$ reactions. This is not surprising since l is, essentially, a geometrical parameter and, as such, can be expected to be determined with reasonable accuracy by relatively low-level ab initio methods, i.e., methods that cannot provide sufficient accuracy in energies but still are suitable for calculation of transition state geometries. Thus, only the UMP2/6-31G(d,p)-level calculations were performed for the other reactions under study and UMP2 values of l were used in the models of reactions 1−5 (Table 2). The values of l obtained display a noticeable decrease upon Cl substitution, changing from 1.414 for reaction 5 to 1.168 for reaction 2b (H abstraction channels) and from 2.191 for reaction 4a to 1.685 for reaction 1 (Cl abstraction channels). Since only the upper one-third of each barrier was fitted with the Eckart formula, the l values provide information not about the barrier as a whole but only about the top region, where most of the tunneling occurs. Units of l are amu$^{1/2}$Å.

TABLE 2: Values of the Reaction "Barrier Width" Parameter (*l*) Used in the Models of Reactions 1−5

reaction		l[a]/amu$^{1/2}$ Å
$H + CHCl_3 \rightarrow H_2 + CCl_3$	(2b)	1.168
$H + CH_2Cl_2 \rightarrow H_2 + CHCl_2$	(3b)	1.276
$H + CH_3Cl \rightarrow H_2 + CH_2Cl$	(4b)	1.371
$H + CH_4 \rightarrow H_2 + CH_3$	(5)	1.414
$H + CCl_4 \rightarrow HCl + CCl_3$	(1)	1.685
$H + CHCl_3 \rightarrow HCl + CHCl_2$	(2a)	1.789
$H + CH_2Cl_2 \rightarrow HCl + CH_2Cl$	(3a)	1.936
$H + CH_3Cl \rightarrow HCl + CH_3$	(4a)	2.191

[a] Reaction "barrier width" parameter obtained from fitting the potential energy profile along IRC with the Eckart formula (see text and Figure 6). For each reaction, only the upper one-third of the barrier was fitted since it is the top part of the barrier that plays the most significant role in the tunneling effect, and therefore, it is more important to describe this upper portion with the Eckart equation than the barrier as a whole.

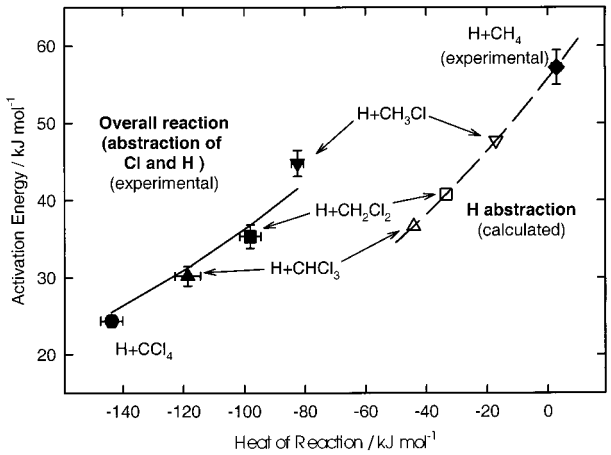

Figure 7. Correlation between activation energies (E_a) and enthalpies (ΔH°_{298}) of reactions 1−5 (see text, subsection III.2). Circle, reaction 1; upward triangles, reaction 2; squares, reaction 3; downward triangles, reaction 4; diamond, reaction 5. Filled symbols, experimental E_a values for the overall reactions and reaction enthalpy values (Cl atom abstraction enthalpy values are used for reactions 1−4). Open symbols and dashed line, E_a for H abstraction computed with the Marcus formula (XIII) using the experimental E_a value for reaction 5 and reaction enthalpy values for H atom abstraction. As can be seen from the plot, the H abstraction channels can be expected to be important in reactions 2−4 since the estimated activation energies for these channels (open symbols, dashed line) are close to the experimental values of the activation energies of the overall reactions (filled symbols).

III.2. Models of Reactions 1−5 and Computation of Reaction Rate Constants. The experimental data obtained in the current work provide no information on individual channels (Cl or H abstraction) in reactions 2−4. Therefore, modeling of these elementary reactions is the only means of assessing the relative importance of the reaction channels. For each overall reaction i ($i = 2-4$), the rate constant of one of the channels can be estimated by means of modeling and that of the other channel can be obtained by subtracting the computed rate from the experimentally measured value of k_i. Since the abstraction of a hydrogen atom from chloromethanes by an H atom is likely to be less efficient than the abstraction of a chlorine atom, we choose to apply modeling to estimation of the rates of these minor channels (2b, 3b, 4b).

The experimental results of the current study demonstrate a correlation between the activation energies of the reactions of H atoms with chlorinated methanes and reaction thermochemistry. Figure 7 presents the dependence of the experimental activation energies of the overall reactions 1−5 on the standard reaction enthalpy values (filled symbols). The enthalpy values for reactions 1−4 used for this plot are those of chlorine atom abstraction (see Table 3 for thermochemical data used in calculations). It is not surprising that a strong correlation (the decrease of the activation energy with increasing reaction exothermicity) is observed for the H + chloromethanes reactions.

TABLE 3: Experimental Values of the Standard Enthalpies of Formation of Species Used in the Models of Reactions 1−5

molecule	ΔH°_{f298}/kJ mol^{-1}	ref
CCl_4	-95.6 ± 1.0	55
$CHCl_3$	-102.7 ± 1.1	55
CH_2Cl_2	-95.0 ± 0.3	55
CH_3Cl	-81.87 ± 0.6	55
CH_4	-74.87 ± 0.34	56
HCl	-92.31 ± 0.10	56
CCl_3	71.13 ± 2.51	57
$CHCl_2$	89.0 ± 3.0	58
CH_2Cl	117.3 ± 3.1	58
CH_3	146.0 ± 1.3	59,60
H	217.999 ± 0.006	56

Numerous efforts have been reported in the literature that were directed at finding a simple relationship between the rates of reactions and thermochemical properties of reactants and products for a series of reactions of similar types (see, for example, refs 61−64). In 1968, Marcus derived an equation relating the reaction barrier E_R and the 0 K energy of reaction ΔH_R specifically for gas-phase reactions of atom transfer[64]

$$E_R = \frac{1}{2}\Delta H_R + E^\circ\left\{1 + (\ln 2)^{-1}\ln\left[\cosh\left(\frac{\Delta H_R \ln 2}{2E^\circ}\right)\right]\right\} \quad \text{(XIII)}$$

Here, E° is the "intrinsic barrier" for a series of similar type reactions ($E_R = E^\circ$ if $\Delta H_R = 0$). Equation XIII, derived by Marcus on the basis of the BEBO method,[65] is very similar in behavior to the Marcus equation for electron-transfer reactions[62]

$$E_R = E^\circ\left(1 + \frac{\Delta H_R}{4E^\circ}\right)^2 \quad \text{(XIV)}$$

at $|\Delta H_R/E^\circ| < 4$ but differs from it outside this region, providing a more realistic limiting behavior for the cases of very large positive and negative ΔH_R. Numerous successful applications of equations XIII and XIV to a variety of series of reactions of similar types have been reported. An update of the literature can be found in the recent article by Blowers and Masel.[66]

The solid line in Figure 7 shows a fit of the experimental activation energy (E_a) versus heat of reaction (ΔH°_{298}) for reactions 1−4 with formula XIII. The fact that the Marcus eq XIII approximately describes the observed correlation provides qualitative support for its application to reactions 1−5, to both Cl and H atom abstraction channels. One can approximately assess the importance of the H abstraction channels by drawing a similar E_a versus ΔH°_{298} dependence (equation XIII, dashed line) through the point representing the $H + CH_4$ reaction (filled diamond). Using the experimental values of the heats of reactions for the hydrogen abstraction channels of reactions 2−4 (2b, 3b, and 4b) and the computed dashed line, one obtains estimates of the activation energies for the reaction channels 2b, 3b, and 4b (shown by the open symbols on the plot). It can be seen from the plot that H abstraction channels are expected to be important in reactions 2−4 since the estimated activation energies for these channels are close to the values of the activation energies of the overall reactions. The differences between the corresponding filled (E_a for overall reactions) and

open (E_a for H abstraction) symbols are only 2.9 kJ mol^{-1} for reaction 2 and 5.4 kJ mol^{-1} for reaction 3.

In all modeling calculations, rate constant values were computed using the transition state theory formula[67]

$$k^{\infty}_{A+B}(T) = \frac{k_B T}{h}\frac{\kappa(T) Q^{\ddagger}}{Q_A Q_B}\exp\left(-\frac{E_R}{k_B T}\right) \qquad \text{(XV)}$$

where $Q^{\ddagger}$, Q_A, and Q_B are partition functions of the transition state and the reactants A and B respectively, E_R is the reaction energy barrier, and $\kappa(T)$ is the temperature-dependent tunneling factor

$$\kappa(T) = \int_{-E_R}^{\infty} P'(E)\exp\left(-\frac{E}{k_B T}\right) dE \qquad \text{(XVI)}$$

Here, $P'(E)$ is the first derivative of the energy-dependent tunneling transition probability $P(E)$, which was calculated using the analytical formula of Eckart[52] (see subsection III.1).

To estimate the rate parameters of the H abstraction channels of reactions 2−4, we first created a model of the reaction of H atoms with methane (reaction 5) and used it to extrapolate the experimentally obtained k_5 temperature dependence to temperatures outside of the experimental range. Frequencies of the transition state and barrier width parameter for H atom abstraction were obtained from the UMP2/6-31G(d,p) ab initio study (see subsection III.1 and Table 2). Four frequencies representing bending deformations of the H$_3$C···H···H transitional structure (doubly degenerate C···H···H bend and CH_3 rock) and the reaction barrier height (E_{R1}) were adjusted to reproduce the experimental rate constant temperature dependence. Vibrational frequencies were adjusted by multiplying all four frequencies by a uniform scaling factor (0.95). The experimental data set reproduced in the calculations consisted of the rate constant values determined in this work and the values of the rate constant for the reverse reaction ($CH_3 + H_2 \rightarrow H + CH_4$, reaction −5) reported by Knyazev et al.[22] For the purpose of data fitting, the values k_{-5} were converted into k_5 via the known reaction thermochemistry (Table 3). It should be noted here that the conversion of k_{-5} into k_5 values performed originally in ref 22 contains an error that appeared due to incorrect temperature values used in the equilibrium constant calculations. The correct k_5 expression from the results of ref 22 is k_5 (T, ref 22) = $5.52 \times 10^{-10}\exp(-7504\ \text{K}/T)$ cm^3 molecule^{-1} s^{-1}.

Figure 8 presents the results of rate constant calculations in comparison with the experimental data of the current and previous studies[22−26] (see Discussion, section IV). The calculated $k_5(T)$ and $k_{-5}(T)$ dependencies (in essence, an extrapolation of the experimental data via transition state theory) can be represented by the following modified Arrhenius expressions in the 298−3000 K temperature region

$$k_5(T) = 7.45 \times 10^{-19}\,T^{2.59}\exp(-5057\ \text{K}/T)\ \text{cm}^3\ \text{molecule}^{-1}\ \text{s}^{-1} \qquad \text{(XVII)}$$

$$k_{-5}(T) = 1.06 \times 10^{-20}\,T^{2.70}\exp(-4451\ \text{K}/T)\ \text{cm}^3\ \text{molecule}^{-1}\ \text{s}^{-1} \qquad \text{(XVIII)}$$

Properties of the transition state, reactants, and products of reaction (5,−5) are listed in Table 4.

The value of the energy barrier of reaction 5 obtained in the fitting of the experimental data is $E_{R1} = 56.00$ kJ mol^{-1}. Within the framework of the Marcus formula, this value of E_{R1} combined with the 0 K reaction enthalpy (energy difference between products and reactants; $\Delta H_{R1} = 0.23$ kJ mol^{-1}) results in the value of the "intrinsic barrier" for H abstraction reactions, $E^{\circ}_H = 55.89$ kJ mol^{-1}.

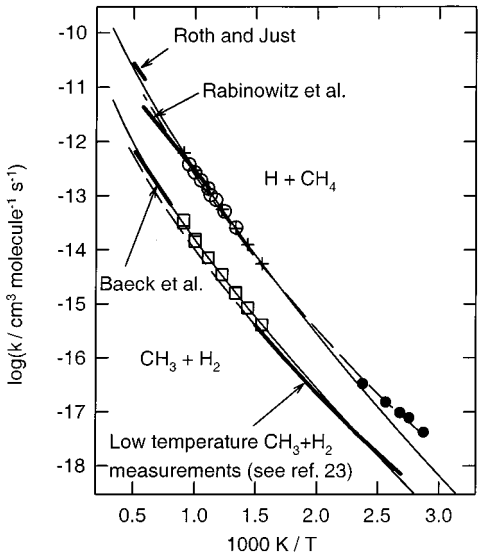

Figure 8. Plot of the rate constants of reactions 5 and −5. Experimental data: open circles, k_5 values obtained in the current study; open squares, experimental k_{-5} values of Knyazev et al.;[22] crosses, the same values[22] converted into k_5 via the reaction thermochemistry; filled circles, k_5 from Marquaire et al.;[23] heavy lines, k_5 values from Roth and Just[26] and Rabinowitz et al.[25] and k_{-5} values from Baeck et al.[24] and several low-temperature measurements analyzed in ref 23. Dashed lines, calculations of Marquaire et al.[23] Solid thin lines, calculations with the model created in the current work.

The rate constants of the H atom abstraction channels in reactions of H atoms with CH_3Cl, CH_2Cl_2, and $CHCl_3$ (reactions 4b, 3b, and 2b) were calculated in an analogous way using the transition state theory formula XV and expression XVI for the tunneling correction coefficient. Reaction energy barriers (listed in Table 4) were obtained from the Marcus eq XIII using the above value of the "intrinsic barrier," $E^{\circ}_H = 55.89$ kJ mol^{-1}. For each reaction transition state, ab initio vibrational frequencies were used (UMP2/6-31G(d,p) scaled by 0.9427[69]), and the four frequencies of the bending deformations of the C···H···H transitional structure were adjusted by the same factor of 0.95 derived from fitting the $k_5(T)$ and $k_{-5}(T)$ experimental data. The reaction models resulted in the temperature dependencies of the rate constants for the direct and the corresponding reverse reactions that can be represented with the following modified Arrhenius expressions within the 298−3000 K temperature interval (units are cm^3 molecule^{-1} s^{-1})

$$k_{2b}(T) \equiv k(H+CHCl_3 \rightarrow H_2+CCl_3) = 3.25 \times 10^{-20}\,T^{2.74}\exp(-2444\ \text{K}/T) \qquad \text{(XIX)}$$

$$k_{-2b}(T) \equiv k(H_2+CCl_3 \rightarrow H+CHCl_3) = 6.36 \times 10^{-24}\,T^{3.51}\exp(-7280\ \text{K}/T) \qquad \text{(XX)}$$

$$k_{3b}(T) \equiv k(H+CH_2Cl_2 \rightarrow H_2+CHCl_2) = 1.52 \times 10^{-19}\,T^{2.66}\exp(-3065\ \text{K}/T) \qquad \text{(XXI)}$$

$$k_{-3b}(T) \equiv k(H_2+CHCl_2 \rightarrow H+CH_2Cl_2) = 3.21 \times 10^{-22}\,T^{3.03}\exp(-6792\ \text{K}/T) \qquad \text{(XXII)}$$

$$k_{4b}(T) \equiv k(H+CH_3Cl \rightarrow H_2+CH_2Cl) = 4.65 \times 10^{-19}\,T^{2.59}\exp(-3847\ \text{K}/T) \qquad \text{(XXIII)}$$

$$k_{-4b}(T) \equiv k(H_2+CH_2Cl \rightarrow H+CH_3Cl) = 1.73 \times 10^{-21}\,T^{2.78}\exp(-5826\ \text{K}/T) \qquad \text{(XXIV)}$$

TABLE 4: Properties of Molecules, Transition States, and Reaction Channels Used in the Models of Reactions 1−5

	Vibrational Frequencies and Degeneracies (cm^{-1})
CCl_4[56]	458, 218(2), 776(3), 314(3)
$CHCl_3$[68]	3034, 680, 363, 1220(2), 774 (2), 261(2)
CH_2Cl_2[68]	299, 1467, 717, 282, 1153, 3040, 898, 1268, 758
CH_3Cl[68]	2937, 3039(2), 1452(2), 1355, 1017(2), 732
H_2[56,a]	4161
HCl[56]	2885
CCl_3[57]	487, 898(2), 266(2), 322[b]
$CHCl_2$[c]	302, 534, 755, 902, 1226, 3138
CH_2Cl[d]	401, 827, 997, 1391, 3101, 3246
CH_3[56]	3002, 580, 3184(2), 1383(2)
H···Cl···$CCl_3^{\ddagger}$[e]	220[175](2), 262[209](2), 299(2), 304, 450, 779, 808(2)
H···Cl···$CHCl_2^{\ddagger}$[e]	244[190], 276[215], 310[241], 323[251], 344, 644, 769, 811, 1125, 1239, 3078
H···Cl···$CH_2Cl^{\ddagger}$[e]	259[209], 284[229], 327[264], 858[692], 786, 788, 1095, 1186, 1418, 3037, 3140
H···Cl···$CH_3^{\ddagger}$[e]	286[230](2), 1038[834](2), 726, 1224, 1427(2), 3004, 3150(2)
H···H···$CCl_3^{\ddagger}$[e]	319[336](2), 1165[1226](2), 261(2), 375, 588, 818(2), 1538
H···H···$CHCl_2^{\ddagger}$[e]	297[313], 336[354], 1112[1170], 1179[1241], 289, 707, 818, 932, 1262, 1587, 3066
H···H···$CH_2Cl^{\ddagger}$[e]	287[302], 506[533], 1134[1194], 1148[1208], 777, 1005, 1028, 1411, 1671, 3029, 3139
H···H···$CH_3^{\ddagger}$[e]	510[537](2), 1075[1132](2), 1073, 1417(2), 1805, 3003, 3158(2)

	Rotational Constants (cm^{-1}) and Symmetry Numbers		
CCl_4[56]	0.05756 (12)	CH_3[56]	7.6036 (6)
$CHCl_3$[f]	0.08670 (3)	H···Cl···$CCl_3^{\ddagger}$[f]	0.05406 (3)
CH_2Cl_2[f]	0.2278 (2)	H···Cl···$CHCl_2^{\ddagger}$[f]	0.08066 (1)
CH_3Cl[f]	1.0159 (3)	H···Cl···$CH_2Cl^{\ddagger}$[f]	0.20228 (1)
H_2[56,a]	59.344 (2)	H···Cl···$CH_3^{\ddagger}$[f]	0.8427 (3)
HCl[56]	10.440 (1)	H···H···$CCl_3^{\ddagger}$[f]	0.08670 (3)
CCl_3[57]	0.08909 (6)[g]	H···H···$CHCl_2^{\ddagger}$[f]	0.19809 (1)
$CHCl_2$[f]	0.26096 (1)	H···H···$CH_2Cl^{\ddagger}$[f]	0.6964 (1)
CH_2Cl[f]	1.34405 (1)	H···H···$CH_3^{\ddagger}$[f]	2.6990 (3)

	Reaction Energy Barriers (kJ mol^{-1}), Degeneracies, and Imaginary Frequencies (cm^{-1})[h]		
$E_1 = 24.35$;	$E_{-1} = 167.10$;	$g = 4$	$\nu_{i,1} = 1007i$
$E_{2a} = 27.96$;	$E_{-2a} = 146.82$;	$g = 3$	$\nu_{i,2a} = 971i$
$E_{3a} = 31.63$;	$E_{-3a} = 131.27$;	$g = 2$	$\nu_{i,3a} = 919i$
$E_{4a} = 37.46$;	$E_{-4a} = 122.33$;	$g = 1$	$\nu_{i,4a} = 848i$
$E_{2b} = 36.04$;	$E_{-2b} = 82.28$;	$g = 1$	$\nu_{i,2b} = 1459i$
$E_{3b} = 39.94$;	$E_{-3b} = 75.80$;	$g = 2$	$\nu_{i,3b} = 1354i$
$E_{4b} = 45.77$;	$E_{-4b} = 67.48$;	$g = 3$	$\nu_{i,4b} = 1277i$
$E_5 = 56.00$;	$E_{-5} = 55.78$;	$g = 4$	$\nu_{i,5} = 1247i$

[a] In calculations of rate constants, partition functions of H_2 were computed by direct summation. Differences between *ortho*- and *para*-H_2 were shown to be negligible. [b] The model of CCl_3 from Hudgens et al.[57] was used. The degree of freedom listed as having vibrational frequency equal to 322 cm^{-1} is an inversion (double well). In calculations of rate constants, the partition function of this inversion was calculated by direct summation over all energy levels (computed in ref 57). [c] Combination of UMP2/6-31G(d,p) calculations scaled[69] by 0.9427 and experimental data from ref 70. [d] Combination of UMP2/6-31G(d,p) calculations scaled[69] by 0.9427 and experimental data from refs 71 and 72. [e] Vibrational frequencies of transition states were obtained in UMP2/6-31G(d,p)-level ab initio calculations and scaled[69] by 0.9427. Frequencies of four transitional modes were adjusted via multiplication by a uniform factor (see text, subsection III.2). Numbers in square brackets are original (unadjusted) scaled ab initio values. [f] From UMP2/6-31G(d,p)-level ab initio calculations. [g] Symmetry factor of 6 is consistent with the treatment of one vibrational mode as double-well inversion (see ref 57 for discussion of rotational symmetry and degeneracy of vibrational levels in relevance to CCl_3). [h] Imaginary frequencies obtained from barrier "width" parameters and fitted values of barrier heights.

These calculated values of the rate constants of the H abstraction channels were subtracted from the experimental values of the rate constants of the overall reactions 2−4 to evaluate the rates of the Cl abstraction channels. The relative contribution of H abstraction in reactions 2−4 decreases with chlorination changing from 42 to 55% (reaction 4) to 15−25% (reaction 3) and 5−10% (reaction 2) in the experimental temperature ranges. This change of the relative importance of H abstraction is in agreement with the trend that can be derived from the changes in ordinate differences between the filled and the open symbols in Figure 7. A discussion of the uncertainties associated with the calculation of H atom abstraction rates and the use of the results for the evaluation of the rate constants of the Cl atom abstraction channels is presented in Section IV.

The temperature-dependent values of the Cl abstraction channels of reactions 1−4 obtained either directly from the experiments (reaction 1) or via applying "corrections" for H abstraction to the experimental rate constant data (reactions 2a, 3a, and 4a) were extrapolated to higher and lower temperatures. This extrapolation was performed by the same modeling method that was described above in relation to the $H + CH_4 \rightarrow H_2 + CH_3$ reaction (reaction 5). Rate constants were calculated using the transition state theory formula (XV). Ab initio (UMP2/6-31G(d,p) level) vibrational frequencies of the corresponding transition states scaled by 0.9427[69] were used. Reaction energy barriers and four vibrational frequencies corresponding to the C···H···H bending deformations were adjusted to reproduce the observed rate constant temperature dependencies. The adjust-

ment of vibrational frequencies was carried out by multiplication by a uniform factor. Optimization was performed by minimizing the sum of squares of deviations of the rate constants. The resultant transition state properties and energy barriers are listed in Table 4.

The values of the frequency adjustment factor that had to be applied to the ab initio frequencies in order to reproduce the observed Cl abstraction rate constants were similar for all four reactions: 1.255 (reaction 1), 1.285 (reaction 2a), 1.240 (reaction 3a), and 1.245 (reaction 4a). This similarity of the four adjustment factors can be expected on the basis of a hypothesis that the same ab initio method applied to four reactions of the same type would overestimate (or underestimate) the force constants of the transitional modes by the same factor.

The reaction models resulted in the temperature dependencies of the rate constants for the direct and the corresponding reverse reactions that can be represented with the following modified Arrhenius expressions within the 298−3000 K temperature interval (units are cm^3 $molecule^{-1}$ s^{-1})

$$k_1(T) \equiv k(H+CCl_4 \rightarrow HCl+CCl_3) = 2.85 \times 10^{-16}\, T^{1.80} \exp(-2062\ K/T) \quad \text{(XXV)}$$

$$k_{-1}(T) \equiv k(HCl+CCl_3 \rightarrow H+CCl_4) = 2.77 \times 10^{-25}\, T^{3.72} \exp(-18686\ K/T) \quad \text{(XXVI)}$$

$$k_{2a}(T) \equiv k(H+CHCl_3 \rightarrow HCl+CHCl_2) = 1.52 \times 10^{-16}\, T^{1.81} \exp(-2472\ K/T) \quad \text{(XXVII)}$$

$$k_{-2a}(T) \equiv k(HCl+CHCl_2 \rightarrow H+CHCl_3) = 1.25 \times 10^{-23}\, T^{3.20} \exp(-16269\ K/T) \quad \text{(XVIII)}$$

$$k_{3a}(T) \equiv k(H+CH_2Cl_2 \rightarrow HCl+CH_2Cl) = 1.38 \times 10^{-16}\, T^{1.79} \exp(-2961\ K/T) \quad \text{(XXIV)}$$

$$k_{-3a}(T) \equiv k(HCl+CH_2Cl \rightarrow H+CH_2Cl_2) = 1.71 \times 10^{-22}\, T^{2.85} \exp(-14296\ K/T) \quad \text{(XXX)}$$

$$k_{4a}(T) \equiv k(H+CH_3Cl \rightarrow HCl+CH_3) = 1.35 \times 10^{-16}\, T^{1.73} \exp(-3755\ K/T) \quad \text{(XXXI)}$$

$$k_{-4a}(T) \equiv k(HCl+CH_3 \rightarrow H+CH_3Cl) = 6.41 \times 10^{-23}\, T^{2.56} \exp(-13236\ K/T) \quad \text{(XXXII)}$$

An attempt was made to model the rate constants of reactions 2−4 without applying any corrections for H atom abstraction, i.e., assuming that Cl atom abstraction is the only process responsible for the experimentally observed overall rate constants. The resultant energy barrier values ($E_{R2} = 28.17$, $E_{R3} = 32.08$, $E_{R4} = 38.17$, units are kJ mol^{-1}) were close to those obtained when H abstraction is taken into account (see Table 4). However, the frequency adjustment factors obtained in this exercise are significantly different for different reactions: 1.255 (1), 1.237 (2), 1.095 (3), and 0.895 (4) (reaction numbers are given in parentheses).

IV. Discussion

IV.1. Experimental Values of the Rate Constants. The current study provides the first direct determination of the temperature dependencies of the rate constants of reactions 1 and 2

$$H + CCl_4 \rightarrow HCl + CCl_3 \quad (1)$$

$$H + CHCl_3 \rightarrow \text{products} \quad (2)$$

Reactions 3−6 have been studied experimentally before

$$H + CH_2Cl_2 \rightarrow \text{products} \quad (3)$$

$$H + CH_3Cl \rightarrow \text{products} \quad (4)$$

$$H + CH_4 \rightarrow H_2 + CH_3 \quad (5)$$

$$H + \textit{iso}\text{-}C_4H_8 \rightarrow \textit{tert}\text{-}C_4H_9 \quad (6)$$

There is agreement between the results of several groups on the rate constant values of reactions 5 and 6.[22−28,73] The most precise determination of $k_6(T)$ is that of Harris and Pitts[28] who used flash photolysis to generate and resonance fluorescence to detect H atoms. A discussion of this and other studies of reaction 6 can be found in ref 44. The values of k_6 obtained in the current work are in good agreement with the results of Harris and Pitts over the experimental temperature interval (Figure 5).

Reactions 5 and −5 have been studied by many groups using a variety of experimental methods. Reviews are available in refs 74, 22−25, and 27 and references therein. Approximate agreement has been reached between the results of different groups, with the exception of the values of k_5 at temperatures above 1700 K, where rate constants obtained by Rabinowitz et al.[25] are lower than those of Roth and Just[26] by a factor of 3.5. An earlier controversy due to the disagreement between k_5/k_{-5} values obtained from experimental data and those calculated from the known thermochemistry of the reaction has been resolved by Marquaire et al.,[23] who studied reaction 5 by the ESR/discharge flow method at temperatures 348−412 K. These authors reproduced their experimental data and those of other groups on reactions 5 and −5 with transition state theory modeling to provide k_5 and k_{-5} temperature dependencies consistent with the thermochemistry of reaction (5,−5). Recently, Knyazev et al.[22] studied the reverse reaction, $CH_3 + H_2 \rightarrow H + CH_4$ (−5) using the laser photolysis/photoionization mass spectrometry experimental method. Experimental data on k_5 obtained in the current study are presented in Figure 8, together with the experimental literature data on reactions 5 and −5 and the values calculated by Marquaire et al.[23] from their model. The experimental data of Roth and Just,[26] Rabinowitz et al.,[25] Marquaire et al.,[23] Baeck et al.,[24] and Knyazev et al.[22] are shown. Also, since the fit of Marquaire et al. provides a near perfect representation of the results of a number of earlier measurements of k_{-5} at relatively low temperatures (see ref 23 for individual data references), the corresponding segment of the calculated curve from ref 23 is shown by a heavy solid line to illustrate these low-temperature data. As can be seen from the plot, the results of the current experimental study are in good agreement with these data and predictions. The differences in calculated curves of the extrapolated $k_5(T)$ and $k_{-5}(T)$ dependencies at low temperatures between ref 23 and the current work are primarily due to slightly different values of the CH_3 enthalpy of formation used in these two studies.

The main motivation for studying reactions 5 and 6 in the current work was a validation of the experimental technique. Reactions 5 and 6 possess very different activation energies and, therefore, different temperature dependencies (Figure 5). Good

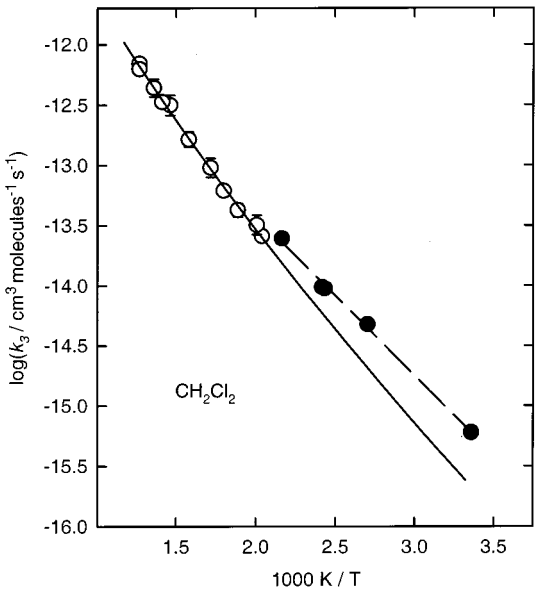

Figure 9. Temperature dependence of the rate constant of reaction 3 ($H + CH_2Cl_2 \rightarrow$ products). Open circles, experimental data obtained in the current study. Filled circles and dashed line, experimental data and Arrhenius fit of Combourieu et al.[16] Solid line, model of reaction 3 created in the current study.

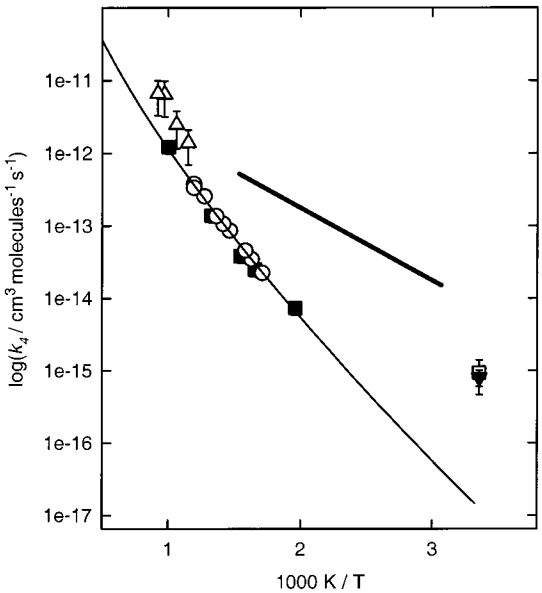

Figure 10. Temperature dependence of the rate constant of reaction 4 ($H + CH_3Cl \rightarrow$ products). Experimental data: open circles, results of the current study; filled squares, Westenberg and deHaas;[18] open triangles, Hart et al.;[17] filled triangle, Jones and Ma;[20] open square, Triebert et al.;[21] heavy solid line, Aders et al.[19] Thin solid line, model created in the current study.

agreement reached between the results of this work and those of other groups on the rate constants of both reactions 5 and 6 confirms the accuracy of the method and the equipment used in the current experiments.

The kinetics of reaction 3 has been studied by Combourieu et al.,[16] who used the discharge flow method with mass spectrometric detection of reactants and products to determine rate constants in the 298−460 K temperature interval. The values of k_3 reported by Combourieu et al. are higher than those calculated via the extrapolation of the experimental data obtained in the current work, on average, by a factor of 2 (Figure 9) and have a somewhat lower activation energy.

Several groups[17−21] reported experimental studies of reaction 4, including three studies where temperature dependencies have been determined.[17−19] The results of these works are in substantial disagreement with each other, with rate coefficients differing by more than an order of magnitude. Figure 10 compares the results of the current study on k_4 with the results of earlier investigations. The values of k_4 obtained in this work are in good agreement with the determination of Westenberg and deHaas,[18] who used the discharge flow method with mass spectrometric detection of CH_3Cl and ESR detection of H atoms. The disagreement with the results of Hart et al.[17] is not very meaningful since these authors used an experimental method ("point source technique" in flames) that yields only approximate rate constant values, as reflected in large uncertainties reported by the authors (Figure 10).

The rate constants of reaction 4 reported by Aders et al.,[19] Jones and Ma,[20] and Triebert et al.[21] are in significant disagreement with those obtained in the current work from the experiments and from extrapolation of experimental data to low temperatures. The values of k_4 from refs 19−21 are larger than the results of this study by 1−3 orders of magnitude.

In refs 18−21, high initial concentrations of H atoms were used (10^{13}−10^{15} atoms cm^{-3}). At the same time, in two of these studies, relatively high concentrations of CH_3Cl were employed ($[CH_3Cl] = (6-84) \times 10^{14}$ molecules cm^{-3} in ref 19; the [CH_3Cl] range was not reported in ref 20 but must have been at least an order of magnitude higher than $[H] \approx 10^{14}$ atoms cm^{-3} since the experiments were conducted under pseudo-first-order conditions for H atoms). Both of these studies employed the fast flow technique with ESR detection of H atoms[19,20] and, in ref 19, mass spectrometric detection of stable species. Although not considered by the authors of these two works, secondary reactions are likely to have significantly influenced the observed values of the rate constants, as described below.

In most earlier studies of reaction 4, Cl atom abstraction was assumed to be the only channel

$$H + CH_3Cl \rightarrow HCl + CH_3 \qquad (4a)$$

However, as shown in section III of the current work, the abstraction of an H atom is likely to be an important channel, reaching approximately 50% of the overall rate constant

$$H + CH_3Cl \rightarrow H_2 + CH_2Cl \qquad (4b)$$

Due to the very high concentrations of H atoms employed in all earlier studies of reaction 4, the reaction of CH_2Cl radicals with H atoms

$$CH_2Cl + H \rightarrow CH_3Cl^* \rightarrow Cl + CH_3 \qquad (7)$$

must be a very fast process. In the initial step of this chemically activated reaction, a highly vibrationally excited CH_3Cl^* molecule is formed. This CH_3Cl^* molecule decomposes into Cl atom and CH_3 radical due to the weaker (compared with C−H) C−Cl bond. Additional production of Cl atoms could occur by reaction of H with HCl

$$H + HCl \rightarrow Cl + H_2 \qquad (8)$$

($k_8 = 2.8 \times 10^{-11} \exp(-2082\ K/T)$ cm^3 molecule^{-1} s^{-1} [75]). Since high ($\sim 10^{15}$ molecules cm^{-3} or higher) concentrations of CH_3Cl were used, the Cl atoms formed in reactions 7 and 8 will react with CH_3Cl (rate constant $k_9 \geq 5 \times 10^{-13}$ cm^3 molecule^{-1} s^{-1} [76]) to produce HCl and CH_2Cl

$$Cl + CH_3Cl \rightarrow HCl + CH_2Cl \qquad (9)$$

Reactions 7−9 form a chain that quickly consumes H atoms and CH_3Cl. Thus, the observed decays of H atoms[20] and CH_3Cl[19] in the experiments of Aders et al.[19] and Jones and Ma[20] did not reflect the rate of reaction 4 but rather the rates of the above chain reaction.

It is impossible to conclude whether a similar process affected the experiments of Triebert et al.[21] because these authors did not report the CH_3Cl concentrations employed in their experiments. In this study (discharge flow technique with mass spectrometric detection of CH_3Cl), significant wall losses of H atoms (first-order wall loss rate constant $k_{H,w} \approx 30-80$ s^{-1}) were reported by the authors who used $k_{H,w}$ as one of the adjustable parameters in fitting the observed $[CH_3Cl]$ versus time data.

The only earlier experimental study of reaction 4 that reported using low concentrations of CH_3Cl was the discharge flow/ESR/mass spectrometry study of Westenberg and deHaas[18] ($[CH_3Cl] \approx 10^{13}$ molecules cm^{-3} as estimated here from a typical $[H] \approx (0.5-2.5) \times 10^{15}$ atoms cm^{-3} and $[H]/[CH_3Cl]$ ratio of 100−250 reported by the authors). It is interesting to note that these authors reported that a much faster reaction was observed if they attempted to conduct experiments with high CH_3Cl concentrations under pseudo-first-order conditions for H atoms. Also, in the experiments performed with an excess of H atoms, Westenberg and deHaas, in some instances, observed a slight decay of H atoms although, due to the high $[H]/[CH_3Cl]$ ratio, H decay would be expected to be negligible. In these cases, reduction of the CH_3Cl concentration resulted in the disappearance of the H atom decay. The authors of ref 18 interpreted these effects as resulting from a hypothetical heterogeneous reactions, that of a fast wall loss of H due to a reaction with absorbed CH_3Cl. However, as can be seen from the above discussion of secondary chemistry, a more likely explanation is the chain process formed by reactions 7−9 when large concentrations of both H and CH_3Cl are used. Since, in the actual k_4 measurements, low CH_3Cl concentrations were used, reaction 8 was not sufficiently fast to influence the CH_3Cl decay, and therefore, the resultant rate constant values were not significantly affected by the secondary reactions. One can estimate from the values of the concentrations used in the experiments of Westenberg and deHaas and the rate constants of reactions 4 and 9 that reaction 9 could account for approximately ≤30% of the overall CH_3Cl decay. However, Cl atom heterogeneous decay, known to be rather efficient on an uncoated glass or quartz surface,[77] could have reduced the influence of reaction 9 on the overall kinetics. As can be seen from the plot in Figure 10, the temperature dependence reported by Westenberg and deHaas coincides with that obtained experimentally in the current study.

The differences between the results of the current determination of the rate constant of reaction 3 ($H + CH_2Cl_2 \rightarrow$ products) and those of Combourieu et al.[16] can be explained by the interference of secondary reactions similar to the kinetic mechanism discussed above for the $H + CH_3Cl$ reaction. In ref 16, experiments to determine k_3 were conducted in an excess of H atoms ($[H] = (0.76-2.14) \times 10^{15}$ atoms cm^{-3}) with moderately high CH_2Cl_2 concentrations ($[CH_2Cl_2] = (2.9-7.7) \times 10^{13}$ molecules cm^{-3}). The sequence of reactions

$$H + CH_2Cl_2 \rightarrow HCl \text{ (or } H_2) + CH_iCl_{3-i} \qquad i = 1, 2 \quad (3)$$

$$H + CH_iCl_{3-i} \rightarrow CH_{i+1}Cl_{3-i}^* \rightarrow CH_{i+1}Cl_{2-i} + Cl \quad (10)$$

$$Cl + CH_2Cl_2 \rightarrow HCl + CHCl_2 \quad (11)$$

can be expected to be sufficiently fast ($k_{11} \geq 3.6 \times 10^{-13}$ cm^3 $molecule^{-1}$ s^{-1} [76]) to result in an effective stoichiometric factor of 2 or larger. For example, at 298 K, the first-order rate of CH_2Cl_2 decay due to reaction 3 in the experiments of Combourieu et al. ($k' = k_3[H]_0 = 6 \times 10^{-16} \times 2.14 \times 10^{15} = 1.28$ s^{-1}; calculated here on the basis of k_3 and $[H]_0$ values reported in ref 16) is comparable to the pseudo-first-order rate of reaction 11 ($k_{11}[Cl] = 3.6 \times 10^{-13} \times 3.9 \times 10^{12} = 1.4$ s^{-1}). Here, the Cl atom concentration was estimated assuming 5% conversion of CH_2Cl_2 in the (slow) reaction 3 and equal efficiency of Cl production. Exact modeling of H and CH_2Cl_2 kinetics under the experimental conditions of ref 16 is not possible because of the likelihood of Cl atom wall loss that would decrease the stoichiometric factor.

The above discussion of the experimental values and temperature dependencies of the rate constants of reactions 1−6 yields the following conclusions. (1) The experimentally observed rates of reactions 5 and 6 (those of H atoms with methane and isobutene) are in excellent agreement with the earlier reported literature data. (2) The temperature dependence of the rate constant of reaction 4 obtained in this work is in agreement with the results of Westenberg and deHaas.[18] (3) Disagreement between the values of k_3 and k_4 obtained in this work and in earlier studies[16,19−21] can be explained by fast secondary reactions that affected the results of the latter.

IV.2. Models of Reactions 1−5. Subsection III.3 describes the method and the results of extrapolation of the experimental values of the rate constants of reactions 1−5 to temperatures outside the experimental ranges and their separation into those of H atom and Cl atom abstraction. The method is based on modeling these reactions within the framework of the transition state theory. Since no experimental information exists on the branching ratios in reactions 2−4, the relative importance of hydrogen and chlorine abstraction was assessed by applying ab initio methods and the Marcus eq XIII which relates reaction barrier to the 0 K enthalpy of reaction (see subsection III.3 and ref 64). First, the rate constants of reaction 5 ($H + CH_4 \rightarrow H_2 + CH_3$) determined in direct experiments were analyzed. The transition state theory model of reaction 5 based on ab initio calculations and fitting of experimental data resulted in the value of the "intrinsic barrier" (to be used within the framework of the Marcus equation) for the reactions of H atom abstraction from substituted methanes by an H atom. Then, rates of H abstraction in reactions 2−4 were calculated on the basis of analogy with reaction 5, using the obtained "intrinsic barrier" value, experimental thermochemistry, and ab initio vibrational frequencies of transition states corrected by a uniform factor derived from modeling of reaction 5. The calculated rates of the H atom abstraction channels (reactions 2b, 3b, and 4b) were subtracted from the experimental values of the rate constants of the overall reactions 2−4 to obtain the rates of the Cl atom abstraction processes. Finally, these rate constants of the reactions of Cl atom abstraction from $CHCl_3$, CH_2Cl_2, CH_3Cl, and CCl_4 (CCl_4 rates were obtained directly from experiments) were reproduced by transition state theory modeling and extrapolated to higher and lower temperatures.

Figure 11 shows the energy barriers obtained in modeling of the Cl and H abstraction channels as a function of the 0 K reaction enthalpies (ΔH_R, products-reactants energy differences). The plot is similar to that in Figure 7. However, the main distinction is that in Figure 11 the Cl and H abstraction channels are fully separated. Also, in Figure 11, energies and barrier heights are plotted instead of standard enthalpies and observed activation energies. Open symbols and the dashed line represent

TABLE 5: Activation Energies (E_a), Preexponential Factors (A), Reaction Degeneracies (g), and Per-Atom Preexponential Factors ($A'=A/g$) Obtained from Reaction Models at 1000 K

reaction		E_a/kJ mol^{-1}	A^a	g	A'^a
$H + CCl_4 \rightarrow HCl + CCl_3$	(1)	32.39	4.749×10^{-10}	4	1.187×10^{-10}
$H + CHCl_3 \rightarrow HCl + CHCl_2$	(2a)	35.88	2.705×10^{-10}	3	9.017×10^{-11}
$H + CH_2Cl_2 \rightarrow HCl + CH_2Cl$	(3a)	39.79	2.078×10^{-10}	2	1.039×10^{-10}
$H + CH_3Cl \rightarrow HCl + CH_3$	(4a)	45.87	1.255×10^{-10}	1	1.255×10^{-10}
$H + CHCl_3 \rightarrow H_2 + CCl_3$	(2b)	43.88	9.798×10^{-11}	1	9.798×10^{-11}
$H + CH_2Cl_2 \rightarrow H_2 + CHCl_2$	(3b)	48.31	2.390×10^{-10}	2	1.195×10^{-10}
$H + CH_3Cl \rightarrow H_2 + CH_2Cl$	(4b)	54.23	4.274×10^{-10}	3	1.425×10^{-10}
$H + CH_4 \rightarrow H_2 + CH_3$	(5)	64.32	6.724×10^{-10}	4	1.681×10^{-10}

[a] Units are cm^3 molecule^{-1} s^{-1}.

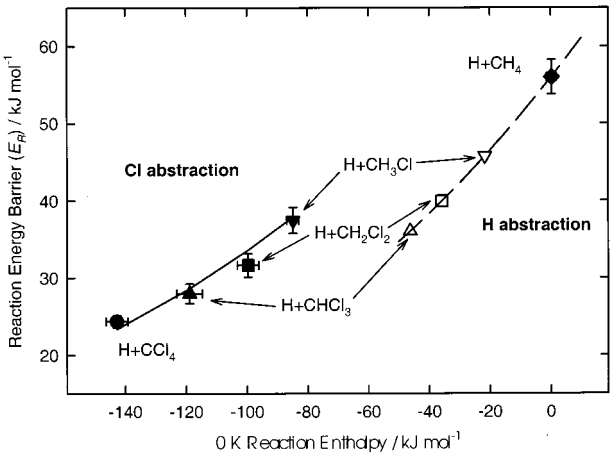

Figure 11. Correlation between the energy barriers (E_R) and the 0 K enthalpies (ΔH_R) of the Cl abstraction channels of reactions 1−5 and the calculated E_R vs ΔH_R dependence for the H abstraction channels (see text, subsection III.2). Curve on the left represents the Cl atom abstraction channels. Curve on the right represents the H atom abstraction channels. Circle, reaction 1; upward triangles, reaction 2; squares, reaction 3; downward triangles, reaction 4; diamond, reaction 5. Filled symbols, E_R values derived from the experimental rate constant data (corrected for H atom abstraction contributions in the cases of reaction 2−4). Open symbols and dashed line, E_R for H abstraction computed with the Marcus formula (XIII) using the "intrinsic barrier" value derived from the model of reaction 5. Solid line, fit of the data on $E_{R,Cl}$ vs $\Delta H_{R,Cl}$ dependence for Cl abstraction with the Marcus formula (XIII).

the values for the H abstraction channels obtained from the calculations via the Marcus equation (eq XIII). Filled symbols indicate E_R (energy barrier) values obtained from modeling experimental data on reactions 1, 2a, 3a, 4a, and 5 (corrected for H abstraction contributions in the cases of reactions 2a, 3a, and 4a). Error limits represent the uncertainties of the experimental activation energies and the standard reaction thermochemistry values. They are shown here to provide an illustration of experimental uncertainties and their influence on the model energetics. The solid line in the left part of the plot represents a Marcus equation (eq XIII) fit of the $E_{R,Cl}$ versus $\Delta H_{R,Cl}$ dependence for Cl abstraction reactions obtained in the modeling. The resultant value of the "intrinsic barrier" is 71.9 kJ mol^{-1}. As can be seen from the quality of the fit, the Marcus equation (eq XIII) provides a good description of the correlation between reaction energy barriers ($E_{R,Cl}$) and 0 K reaction enthalpy ($\Delta H_{R,Cl}$) for Cl abstraction.

In the modeling of the Cl abstraction reactions, the values of the frequency adjustment factor that had to be applied to ab initio frequencies of the transitional modes in order to reproduce the observed rate constants were very similar for all four reactions considered. As was discussed in subsection III.3, one can expect such similarity if one assumes that a particular ab initio method results in approximately similar errors when used to compute force constants of transitional modes in a series of reactions of the same type. The similarity of the obtained adjustment factors and the good representation of the E_R versus ΔH_R dependence with the Marcus equation demonstrate the internal coherence of the model. On the other hand, if no correction for the H atom abstraction channels is introduced and the experimental rate constants of reactions 2−4 are reproduced with transition state theory models assuming that Cl abstraction is the only existing channel, the frequency adjustment factors obtained in the process of tuning the models' parameters demonstrate rather inconsistent behavior. These factors differ significantly for reactions 1−4, changing from 1.255 (reaction 1) to 0.895 (reaction 4), demonstrating the lesser plausibility of such models.

Although the models of both the H and the Cl abstraction channels created in this work appear to be internally coherent and agree with the experimental data (upon which they are based), one should emphasize the approximate nature of the calculated H atom abstraction rates in reactions 2−4. The uncertainties in these rate constant values originate in the use of the Marcus equation to predict (extrapolate) reaction barriers and in the frequency adjustment factor derived from the data on the $H + CH_4$ reaction. Since the Cl atom abstraction rates in reactions 2−4 are obtained by subtracting the calculated rates of H abstraction from the experimental values for the overall reactions, the uncertainties of calculations propagate into the values of rate constants of the Cl abstraction channels. These uncertainties are the highest for reaction 4, where the H and the Cl abstraction channels have comparable importance. Reactions 2a and 3a are affected to a lesser extent. Of course, models of reactions 1 and 5 are not affected by any of these sources of uncertainties. Extrapolation to temperatures outside of the experimental ranges was performed with the use of transition state theory with a tunneling contribution calculated using a rather simple one-dimensional model. Any application of these results should be performed with the awareness of the uncertainties inherent to the models and theories used.

The models of reactions 1−5 developed in the current study on the basis of experimental data and ab initio calculations indicate important roles of abstraction of H atoms in the H + chloromethanes reactions. This conclusion is in agreement with Tsang,[15] who argued that H abstraction in H + chloromethanes can be of significant importance. Tsang based his analysis on the results of Clark and Tedder,[78] who studied reactions of H atoms with a series of halogenomethanes by end product analysis.

Table 5 presents the activation energies (E_a) and preexponential factors (A) for H and Cl atom abstraction channels obtained from the models of reactions 1−5 developed in this study. These Arrhenius parameters were computed at a fixed temperature of 1000 K. Due to the curvature in Arrhenius coordinates exhibited by the rate constants, the values of E_a

and A in Table 5 are noticeably different from those derived from the temperature dependencies of the experimental rate constants (expressions V−IX). Also present in Table 5 are the reaction degeneracy factors (calculated following the method of refs 79−81 and coinciding, for the reactions considered here, with the numbers of atoms subject to abstraction) and the "per-atom" preexponential factors A' obtained by dividing A by the reaction degeneracy. As can be seen from the data, A' values for Cl abstraction are approximately the same for all chloromethanes while those for H atom abstraction decrease with increasing chlorination (e.g., A' for chloroform is lower than that for methane by a factor of 1.7).

V. Summary

Reactions of H atoms with methane, four chlorinated methanes, and isobutene have been studied experimentally with the discharge flow/resonance fluorescence technique over wide ranges of temperatures and at low pressures.

$$H + CCl_4 \rightarrow HCl + CCl_3 \quad (1)$$

$$H + CHCl_3 \rightarrow \text{products} \quad (2)$$

$$H + CH_2Cl_2 \rightarrow \text{products} \quad (3)$$

$$H + CH_3Cl \rightarrow \text{products} \quad (4)$$

$$H + CH_4 \rightarrow H_2 + CH_3 \quad (5)$$

$$H + \textit{iso}\text{-}C_4H_8 \rightarrow \textit{tert}\text{-}C_4H_9 \quad (6)$$

The resultant rate constants can be represented with the Arrhenius expressions (experimental temperature ranges are given in parentheses)

$$k_1 = (1.36 \pm 0.31) \times 10^{-10} \exp(-2937 \pm 92\ \text{K}/T)\ \text{cm}^3\ \text{molecule}^{-1}\ \text{s}^{-1}\ (297-904\text{K}) \quad (V)$$

$$k_2 = (1.33 \pm 0.43) \times 10^{-10} \exp(-3640 \pm 154\ \text{K}/T)\ \text{cm}^3\ \text{molecule}^{-1}\ \text{s}^{-1}\ (417-854\text{K}) \quad (VI)$$

$$k_3 = (1.43 \pm 0.50) \times 10^{-10} \exp(-4250 \pm 184\ \text{K}/T)\ \text{cm}^3\ \text{molecule}^{-1}\ \text{s}^{-1}\ (491-787\text{K}) \quad (VII)$$

$$k_4 = (2.24 \pm 0.75) \times 10^{-10} \exp(-5394 \pm 202\ \text{K}/T)\ \text{cm}^3\ \text{molecule}^{-1}\ \text{s}^{-1}\ (586-839\text{K}) \quad (VIII)$$

$$k_5 = (2.55 \pm 0.89) \times 10^{-10} \exp(-6874 \pm 267\ \text{K}/T)\ \text{cm}^3\ \text{molecule}^{-1}\ \text{s}^{-1}\ (748-1054\text{K}) \quad (IX)$$

$$k_6 = (4.57 \pm 1.32) \times 10^{-11} \exp(-729 \pm 92\ \text{K}/T)\ \text{cm}^3\ \text{molecule}^{-1}\ \text{s}^{-1}\ (299-503\text{K}) \quad (X)$$

Error limits in expressions V−X represent uncertainties of the fits only and are reported as 2σ.

Transition state theory models of reactions 1−5 were created on the basis of ab initio calculations, the Marcus expression for correlation between reaction barriers and energetics, and analysis of experimental data. It is demonstrated that the Marcus-expression-based formalism adequately describes the observed temperature dependencies of the rate constants of the overall reactions. According to the models, abstraction of H atoms in reactions 2−4 is an important process accounting for 5−55% of the overall rate constants under the experimental conditions. The models result in the expressions for the rate constants of the Cl abstraction (reactions 1, 2a, 3a, and 4a) and the H abstraction (reactions 2b, 3b, 4b, and 5) channels and the corresponding reverse reactions over wide range of temperatures (298−3000 K)

$$k_1(T) \equiv k(H+CCl_4 \rightarrow HCl+CCl_3) = 2.85 \times 10^{-16}\, T^{1.80} \exp(-2062\ \text{K}/T) \quad (XXV)$$

$$k_{-1}(T) \equiv k(HCl+CCl_3 \rightarrow H+CCl_4) = 2.77 \times 10^{-25}\, T^{3.72} \exp(-18686\ \text{K}/T) \quad (XXVI)$$

$$k_{2a}(T) \equiv k(H+CHCl_3 \rightarrow HCl+CHCl_2) = 1.52 \times 10^{-16}\, T^{1.81} \exp(-2472\ \text{K}/T) \quad (XXVII)$$

$$k_{-2a}(T) \equiv k(HCl+CHCl_2 \rightarrow H+CHCl_3) = 1.25 \times 10^{-23}\, T^{3.20} \exp(-16269\ \text{K}/T) \quad (XXVIII)$$

$$k_{3a}(T) \equiv k(H+CH_2Cl_2 \rightarrow HCl+CH_2Cl) = 1.38 \times 10^{-16}\, T^{1.79} \exp(-2961\ \text{K}/T) \quad (XXIX)$$

$$k_{-3a}(T) \equiv k(HCl+CH_2Cl \rightarrow H+CH_2Cl_2) = 1.71 \times 10^{-22}\, T^{2.85} \exp(-14296\ \text{K}/T) \quad (XXX)$$

$$k_{4a}(T) \equiv k(H+CH_3Cl \rightarrow HCl+CH_3) = 1.35 \times 10^{-16}\, T^{1.73} \exp(-3755\ \text{K}/T) \quad (XXXI)$$

$$k_{-4a}(T) \equiv k(HCl+CH_3 \rightarrow H+CH_3Cl) = 6.41 \times 10^{-23}\, T^{2.56} \exp(-13236\ \text{K}/T) \quad (XXXII)$$

$$k_{2b}(T) \equiv k(H+CHCl_3 \rightarrow H_2+CCl_3) = 3.25 \times 10^{-20}\, T^{2.74} \exp(-2444\ \text{K}/T) \quad (XIX)$$

$$k_{-2b}(T) \equiv k(H_2+CCl_3 \rightarrow H+CHCl_3) = 6.36 \times 10^{-24}\, T^{3.51} \exp(-7280\ \text{K}/T) \quad (XX)$$

$$k_{3b}(T) \equiv k(H+CH_2Cl_2 \rightarrow H_2+CHCl_2) = 1.52 \times 10^{-19}\, T^{2.66} \exp(-3065\ \text{K}/T) \quad (XXI)$$

$$k_{-3b}(T) \equiv k(H_2+CHCl_2 \rightarrow H+CH_2Cl_2) = 3.21 \times 10^{-22}\, T^{3.03} \exp(-6792\ \text{K}/T) \quad (XXII)$$

$$k_{4b}(T) \equiv k(H+CH_3Cl \rightarrow H_2+CH_2Cl) = 4.65 \times 10^{-19}\, T^{2.59} \exp(-3847\ \text{K}/T) \quad (XXIII)$$

$$k_{-4b}(T) \equiv k(H_2+CH_2Cl \rightarrow H+CH_3Cl) = 1.73 \times 10^{-21}\, T^{2.78} \exp(-5826\ \text{K}/T) \quad (XXIV)$$

$$k_5(T) \equiv k(H+CH_4 \rightarrow H_2+CH_3) = 7.45 \times 10^{-19}\, T^{2.59} \exp(-5057\ \text{K}/T) \quad (XVII)$$

$$k_{-5}(T) \equiv k(H_2+CH_3 \rightarrow H+CH_4) = 1.06 \times 10^{-20}\, T^{2.70} \exp(-4451\ \text{K}/T) \quad (XVIII)$$

Acknowledgment. This research was supported by the National Science Foundation, Combustion and Thermal Plasmas Program under Grant CTS-9807136. The authors would like to thank Dr. L. J. Stief for helpful advice and the loan of equipment and Dr. V. L. Orkin for advice and help with the analyses of chloromethane samples.

Supporting Information Available: Results of the ab initio calculations of the transition states, reactants, and products of

reaction 1−5; information on the optimized geometries and energies of these species (10 pages).

References and Notes

(1) Karra, S. B.; Gutman, D.; Senkan, S. M. *Combust. Sci. Technol.* **1988**, *60*, 45.
(2) Chang, W. D.; Senkan, S. M. *Environ. Sci. Technol.* **1989**, *23*, 442.
(3) Lee, K. Y.; Puri, I. K. *Combust. Flame* **1993**, *92*, 440.
(4) Lee, K. Y.; Puri, I. K. *Combust. Flame* **1993**, *94*, 191.
(5) Lee, K. Y.; Yang, M. H.; Puri, I. K. *Combust. Flame* **1993**, *92*, 419.
(6) Taylor, P. H.; Tirey, D. A.; Dellinger, B. *Combust. Flame* **1996**, *104*, 260.
(7) Taylor, P. H.; Tirey, D. A.; Dellinger, B. *Combust. Flame* **1996**, *106*, 1.
(8) Wang, H.; Hahn, T. O.; Sung, C. J.; Law, C. K. *Combust. Flame* **1996**, *105*, 291.
(9) Ho, W. P.; Yu, Q.-R.; Bozzelli, J. W. *Combust. Sci. Technol.* **1992**, *85*, 23.
(10) Chang, W. D.; Karra, S. B.; Senkan, S. M. *Combust. Sci. Technol.* **1986**, *49*, 107.
(11) Xieqi, M.; Cicek, B.; Senkan, S. M. *Combust. Flame* **1993**, *94*, 131.
(12) Cicek, B.; Senkan, S. M. *Combust. Sci. Technol.* **1993**, *91*, 53.
(13) Cui, J. P.; He, Y. Z.; Tsang, W. *J. Phys. Chem.* **1989**, *93*, 724.
(14) Karra, S. B.; Senkan, S. M. *Combust. Sci. Technol.* **1987**, *54*, 333.
(15) Tsang, W. *Combust. Sci. Technol.* **1990**, *74*, 99.
(16) Combourieu, J.; Le Bras, G.; Paty, C. *Symp. Int. Combust. Proc.* **1973**, *14*, 485.
(17) Hart, L. W.; Grunfelder, C.; Fristrom, R. M. *Combust. Flame* **1974**, *23*, 109.
(18) Westenberg, A. A.; deHaas, N. *J. Chem. Phys.* **1975**, *62*, 3321.
(19) Aders, W.-K.; Pangritz, D.; Wagner, H. Gg. *Ber. Bunsen-Ges. Phys. Chem.* **1975**, *79*, 90.
(20) Jones, W. E.; Ma, J. L. *Can. J. Chem.* **1986**, *64*, 2192.
(21) Triebert, J.; Meinike, T.; Olzmann, M.; Scherzer, K. *Z. Phys. Chem. (Munich)* **1995**, *191*, 47.
(22) Knyazev, V. D.; Bencsura, A.; Stoliarov, S. I.; Slagle, I. R. *J. Phys. Chem.* **1996**, *100*, 11346.
(23) Marquaire, P.-M.; Dastidar, A. G.; Manthorne, K. C.; Pacey, P. D. *Can. J. Chem.* **1994**, *72*, 600.
(24) Baeck, H. J.; Shin, K. S.; Yang, H.; Qiun, Z.; Lissianski, V.; Gardiner, W. C., Jr. *J. Phys. Chem.* **1995**, *99*, 15925.
(25) Rabinowitz, M. J.; Sutherland, J. W.; Patterson, P. M.; Klemm, R. B. *J. Phys. Chem.* **1991**, *95*, 674.
(26) Roth, P.; Just, Th. *Ber. Bunsen-Ges. Phys. Chem.* **1975**, *79*, 682.
(27) Baulch, D. L.; Cobos, C. J.; Cox, R. A.; Esser, C.; Frank, P.; Just, Th.; Kerr, J. A.; Pilling, M. J.; Troe, J.; Walker, R. W.; Warnatz, J. *J. Phys. Chem. Ref. Data* **1992**, *21*, 411.
(28) Harris, G. W.; Pitts, J. N. J. *J. Chem. Phys.* **1982**, *77*, 3994.
(29) Certain commercial instruments and materials are identified in this article to adequately specify the procedures. In no case does such identification imply recommendation or endorsement by NIST, nor does it imply that the instruments or materials are necessarily the best available for this purpose.
(30) Kaufman, F. *Prog. React. Kinet.* **1961**, *1*, 1.
(31) Poirier, R. V.; Carr, R. W. *J. Phys. Chem.* **1971**, *75*, 1593.
(32) Ogren, P. J. *J. Phys. Chem.* **1975**, *79*, 1749.
(33) Howard, C. J. *J. Phys. Chem.* **1979**, *83*, 3.
(34) Sepehrad, A.; Marshall, R. M.; Purnell, H. *Int. J. Chem. Kinet.* **1979**, *11*, 411.
(35) Davis, D. D.; Braun, W. *Appl. Opt.* **1968**, *7*, 2071.
(36) Okabe, H. *Photochemistry of Small Molecules.*; Wiley: New York, 1978.
(37) Kurylo, M. J.; Peterson, N. C.; Braun, W. *J. Chem. Phys.* **1970**, *53*, 2776.
(38) Tsang, W.; Herron, J. T. *J. Phys. Chem. Ref. Data* **1991**, *20*, 609.
(39) Lambert, M.; Sadowski, C. M.; Carrington, T. *Int. J. Chem. Kinet.* **1985**, *17*, 685.
(40) Krasnoperov, L. N.; Kalinovski, I. J.; Chu, H.-N.; Gutman, D. *J. Phys. Chem.* **1993**, *97*, 11787.
(41) Kartoshkin, V. A.; Klementev, G. V.; Melnikov, V. D. *Opt. Spektrosk.* **1983**, *55*, 606.
(42) Zelenov, V. V.; Kukui, A. S.; Dodonov, A. F. *Khim Fiz.* **1986**, *5*, 702.
(43) Redsun, S. G.; Knize, R. J. *Phys. Rev. A* **1988**, *37*, 737.
(44) Knyazev, V. D.; Dubinsky, I. A.; Slagle, I. R.; Gutman, D. *J. Phys. Chem.* **1994**, *98*, 5279.
(45) Bevington, P. R. *Data Reduction and Error Analysis for the Physical Sciences*; McGraw-Hill: New York, 1969.
(46) Frisch, M. J.; Trucks, G. W.; Schlegel, H. B.; Gill, P. M. W.; Johnson, B. G.; Robb, M. A.; Cheeseman, J. R.; Keith, T.; Petersson, G. A.; Montgomery, J. A.; Raghavachari, K.; Al-Laham, M. A.; Zakrzewski, V. G.; Ortiz, J. V.; Foresman, J. B.; Cioslowski, J.; Stefanov, B. B.; Nanayakkara, A.; Challacombe, M.; Peng, C. Y.; Ayala, P. Y.; Chen, W.; Wong, M. W.; Andres, J. L.; Replogle, E. S.; Gomperts, R.; Martin, R. L.; Fox, D. J.; Binkley, J. S.; Defrees, D. J.; Baker, J.; Stewart, J. P.; Head-Gordon, M.; Gonzalez, C.; Pople, J. A. *Gaussian 94*, Revision E.1; Gaussian, Inc.: Pittsburgh, PA, 1995.
(47) Kurosaki, Y.; Takayanagi, T. *J. Chem. Phys.* **1999**, *110*, 10830.
(48) Maity, D. K.; Duncan, W. T.; Truong, T. N. *J. Phys. Chem. A* **1999**, *103*, 2152.
(49) Knyazev, V. D.; Slagle, I. R. *J. Phys. Chem.* **1996**, *100*, 16899.
(50) Fukui, K. *Acc. Chem. Res.* **1981**, *14*, 363.
(51) Gonzalez, C.; Schlegel, H. B. *J. Phys. Chem.* **1990**, *94*, 5523.
(52) Eckart, C. *Phys. Rev.* **1930**, *35*, 1303.
(53) Schlegel, H. B. *J. Chem. Phys.* **1986**, *84*, 4530.
(54) Schlegel, H. B. *J. Phys. Chem.* **1988**, *92*, 3075.
(55) In *Thermodynamic Properties of Individual Substances*; Gurvich, L. V., Veyts, I. V., Alcock, C. B., Eds.; Hemisphere: New York, 1992; Vol. 2.
(56) Chase, M. W., Jr. *J. Phys. Chem. Ref. Data* **1998**, *Monograph 9*, 1.
(57) Hudgens, J. W.; Johnson, R. D. I.; Timonen, R. S.; Seetula, J. A.; Gutman, D. *J. Phys. Chem.* **1991**, *95*, 4400.
(58) Seetula, J. A. *J. Chem. Soc., Faraday Trans.* **1996**, *92*, 3069.
(59) Kerr, J. A. In *CRC Handbook of Chemistry and Physics*; Lide, D. R., Ed.; CRC Press: Boca Raton, FL, 1994.
(60) Seetula, J. A.; Russell, J. J.; Gutman, D. *J. Am. Chem. Soc.* **1990**, *112*, 1347.
(61) Evans, M. G.; Polanyi, M. *Trans. Faraday Soc.* **1938**, *34*, 11.
(62) Marcus, R. A. *J. Chem. Phys.* **1955**, *24*, 966.
(63) Semenov, N. N. *Some Problems of Chemical Kinetics and Reactivity*; Pergamon Press Inc.: New York, 1958.
(64) Marcus, R. A. *J. Chem. Phys.* **1968**, *72*, 891.
(65) Johnson, H. S. *Adv. Chem. Phys.* **1960**, *3*, 131.
(66) Blowers, P.; Masel, R. I. *J. Phys. Chem. A* **1999**, *103*, 7047.
(67) Johnston, H. S. *Gas Phase Reaction Rate Theory*; The Ronald Press: New York, 1966.
(68) Shimanouchi, T. *Tables of Molecular Vibrational Frequencies. Consolidated Volume I.*; National Bureau of Standards: Gaithersburg, MD, 1972.
(69) Pople, J. A.; Scott, A. P.; Wong, M. W.; Radom, L. *Isr. J. Chem.* **1993**, *33*, 345.
(70) Carver, T. G.; Andrews, L. *J. Chem. Phys.* **1969**, *50*, 4235.
(71) Andrews, L.; Smith, D. W. *J. Chem. Phys.* **1970**, *53*, 2956.
(72) Jacox, M. E.; Milligan, D. E. *J. Chem. Phys.* **1970**, *53*, 2688.
(73) Canosa, C. E.; Marshall, R. M. *Int. J. Chem. Kinet.* **1981**, *13*, 303.
(74) Tsang, W.; Hampson, R. F. *J. Phys. Chem. Ref. Data* **1986**, *15*, 1087.
(75) Adusei, G. Y.; Fontijn, A. *Symp. Int. Combust. Proc.* **1994**, *25*, 801.
(76) Atkinson, R.; Baulch, D. L.; Cox, R. A.; Hampson, R. F., Jr.; Kerr, J. A.; Rossi, M. J.; Troe, J. *J. Phys. Chem. Ref. Data* **1997**, *26*, 521.
(77) Ogryzlo, E. A. *Can. J. Chem.* **1961**, *39*, 2556.
(78) Clark, D. T.; Tedder, J. M. *Trans. Faraday Soc.* **1966**, *62*, 405.
(79) Pechukas, P. In *Dynamics of Molecular Collisions*; Miller, W. H., Ed.; Plenum Press: New York, 1976; Vol. B.
(80) Karas, A. J.; Gilbert, R. G.; Collins, M. A. *Chem. Phys. Lett.* **1992**, *193*, 181.
(81) Gilbert, R. G.; Smith, S. C. *Theory of Unimolecular and Recombination Reactions*; Blackwell: Oxford, 1990.